environments

MDPI

Article

Seasonal Variability of Potentially Toxic Elements (PTEs) in Road Dust from Mexico City: Source Identification, Particle Characterization, and Lung Bioaccessibility

Benedetto Schiavo [1,*], Diana María Meza-Figueroa [2,*], Claudio Inguaggiato [3], Ofelia Morton-Bermea [1], Daisy Valera-Fernández [4], Belem González-Grijalva [2], Francisco Berrellez-Reyes [2] and Elizabeth Hernández-Álvarez [1]

[1] Instituto de Geofísica, Universidad Nacional Autónoma de México, Mexico City 04150, Mexico; omorton@igeofisica.unam.mx (O.M.-B.); aeliza@igeofisica.unam.mx (E.H.-Á.)
[2] Departamento de Geología, Universidad de Sonora, Hermosillo 83000, Mexico; belem.gonzalez@unison.mx (B.G.-G.); francisco.berrellez@unison.mx (F.B.-R.)
[3] Departamento de Geología, Centro de Investigación Científica y de Educación Superior de Ensenada, Baja California (CICESE), Ensenada 22860, Mexico; inguaggiato@cicese.edu.mx
[4] Instituto de Geología, Universidad Nacional Autónoma de México, Mexico City 04150, Mexico; daisyvalera@geologia.unam.mx
* Correspondence: benedetto@igeofisica.unam.mx (B.S.); diana.meza@unison.mx (D.M.M.-F.)

Abstract

Road dust is an important urban reservoir of potentially toxic elements (PTEs) and a relevant source of human exposure through resuspension and inhalation, particularly in large megacities. This study provides an integrated assessment of the seasonal variability, contamination levels, source identification, particle characteristics, lung bioaccessibility, and health risk of road dust in Mexico City, one of the world's largest urban centers. A total of 74 road dust samples were collected during the dry and wet seasons, and V, Cr, Mn, Co, Ni, Cu, As, Cd, Sb, and Pb were analyzed by ICP–MS in the <20 μm fraction. Geochemical indices, spatial analysis, Pearson correlation, principal component analysis, SEM–EDS particle characterization, in vitro lung bioaccessibility (ALF), and human health risk models were applied. Sb, Cu, and Pb were identified as the most enriched elements, exceeded local background concentrations at all sampling sites. Spatial patterns revealed recurrent hotspots in the northern, northeastern, and central sectors of the city. SEM–EDS analyses showed that most particles belonged to the 2.5–5 μm equivalent-size class and included Fe-rich spherules, Pb-rich aggregates, silicate grains, and C-rich particles. Health risk assessment indicated acceptable risks for adults, whereas children exceeded the non-carcinogenic threshold (HI = 3.85–4.60) and slightly surpassed the upper acceptable carcinogenic risk level. Lung bioaccessibility results revealed low Pb solubility but high mobility of Ni and Cu, with some samples reaching complete dissolution under ALF conditions. These findings demonstrate that traffic-derived road dust represents a persistent urban exposure pathway in Mexico City and highlight the importance of integrating total concentrations, particle characteristics, and bioaccessibility data to improve environmental and health-risk assessments in urban environments.

Keywords: trace metals; spatial distribution; health risk assessment; ICP-MS; SEM-EDS

Check for updates

Academic Editor: Daniele Fattorini

Received: 12 May 2026
Revised: 23 June 2026
Accepted: 23 June 2026
Published: 1 July 2026

Copyright: © 2026 by the authors. Licensee MDPI, Basel, Switzerland. This article is an open access article distributed under the terms and conditions of the Creative Commons Attribution (CC BY) license.

1. Introduction

Urban environments are increasingly recognized as complex systems where natural and anthropogenic processes converge, leading to the accumulation of particles enriched

in potentially toxic elements (PTEs). Among the different environmental compartments, road dust has emerged as a critical medium due to its dual role as both a sink and a secondary source of contaminants, integrating inputs from atmospheric deposition, vehicular emissions, industrial activities, and urban infrastructure degradation [1–3]. As a result, road dust provides a spatially integrated record of urban pollution and represents a key interface between environmental contamination and human exposure.

Road dust is composed of a heterogeneous mixture of geogenic mineral particles, organic matter, and anthropogenic debris, including residues from brake and tire wear, fuel combustion, and construction materials [1,4]. These particles span a wide range of sizes, from coarse fractions to fine and ultrafine particles capable of remaining suspended and being readily inhaled [5]. In particular, fine and ultrafine fractions are of major concern due to their ability to penetrate deep into the respiratory system and reach the alveolar region [6,7]. The continuous resuspension of road dust by traffic and wind further enhances its relevance as a source of airborne exposure in urban environments [8].

The accumulation of PTEs such as Pb, Cd, Cu, Ni, among others in road dust is widely documented and represents a major environmental and public health concern due to their persistence, non-biodegradable nature, and toxicity [2,3]. These elements originate from both natural and anthropogenic sources, although urban settings are typically dominated by anthropogenic inputs, particularly those associated with traffic emissions, industrial processes, and fossil fuel combustion [1,4,9]. Once deposited, PTEs can be remobilized through resuspension or redistributed via runoff, contributing to the contamination of air, soils, and water systems [1,10]. In this context, road dust is not only a passive reservoir but also an active component of urban pollution dynamics. Exposure to PTEs associated with urban dust has been linked to a wide range of adverse health effects, including respiratory and cardiovascular diseases, neurological impairment, and carcinogenic outcomes [2,9]. These effects are largely driven by the ability of transition metals to catalyze the formation of reactive oxygen species (ROS), inducing oxidative stress and cellular damage [2]. Prolonged exposure may therefore contribute to chronic health conditions and increased morbidity in urban populations [11]. Children are particularly vulnerable due to their physiological susceptibility and exposure patterns, often showing higher non-carcinogenic and carcinogenic risks compared to adults [12,13].

Seasonal variability plays a fundamental role in controlling the accumulation, redistribution, and chemical behavior of PTEs in urban dust [11]. Climatic factors such as precipitation, temperature, and wind patterns influence both the generation and removal of PM, leading to significant temporal differences in metal concentrations. During dry periods, enhanced dust resuspension and limited washout favor the accumulation of PTEs, whereas during wet conditions, rainfall promotes particle removal and redistribution across environmental compartments [14–16]. In semiarid environments, these seasonal contrasts can be particularly pronounced, with pre- and post-monsoon conditions showing substantial differences not only in total metal concentrations but also in their geochemical behavior and associated health risks [17]. Recent studies have shown that seasonal variability extends beyond bulk concentrations and may also influence metal bioaccessibility through changes in particle composition, mineralogical phases, and surface reactivity [17,18]. Bioaccessibility is particularly relevant because it reflects the fraction of metals that can be mobilized under physiological conditions [19], including simulated lung fluids such as Gamble solution and artificial lysosomal fluid [20]. Furthermore, particle size and morphology exert a critical control on both transport and toxicity, as finer and irregular particles exhibit higher surface area and reactivity, enhancing their interaction with biological systems [6].

Despite the growing number of studies on urban dust contamination, important knowledge gaps remain. Many investigations focus exclusively on total concentrations

without incorporating bioaccessibility, potentially leading to inaccurate assessments of health risks [21,22]. Furthermore, studies simultaneously evaluating seasonal variability, source identification, particle characteristics, lung bioaccessibility, and health risks within a single framework remain limited [18], particularly for road dust in large megacities with complex emission sources. Addressing these gaps is essential for improving our understanding of urban pollution processes and their implications for human health. Mexico City, one of the largest megacities in the world, represents a particularly relevant case study due to its high population density, intense vehicular activity, and complex emission sources [23]. The strong contrast between dry and rainy seasons further enhances the variability of dust accumulation and redistribution processes, creating a highly dynamic environment for PTE behavior. However, integrated studies addressing seasonal variability, contamination levels, source identification, bioaccessibility, and particle morphology in this region remain scarce.

Therefore, the aim of this study was to provide an integrated assessment of seasonal variability, contamination levels, source identification, particle characteristics, lung bioaccessibility, and human health risks associated with PTEs in Mexico City road dust. Specifically, the objectives were: (i) to determine the seasonal differences in PTE concentrations in road dust collected in wet and dry season; (ii) to evaluate the level of contamination using multiple geochemical indices; (iii) to identify the potential sources of pollution; (iv) to characterize the morphology and composition of dust particles using SEM–EDS; and (v) to assess the degree of lung bioaccessibility and associated human health risks in order to better understand their origin, behavior, and potential toxicity.

2. Materials and Methods

2.1. Study Area

Mexico City, the capital of Mexico, is one of the largest and most densely populated megacities in the world, with more than 20 million inhabitants in its metropolitan area (Figure 1). Within the administrative boundaries of Mexico City, the population is approximately 9.2 million inhabitants according to the most recent national census [24]. The city covers an area of approximately 1485 km^2 and is located between 19°03′–19°36′ N and 98°57′–99°22′ W, at an average elevation of about 2240 m above sea level. The basin is surrounded by mountain ranges, with elevation increasing from north to south, which restricts atmospheric circulation and favors the accumulation of airborne particles and surface dust.

The climate of Mexico City is classified as temperate sub-humid, characterized by two well-defined seasons: a dry season extending from November to April and a wet season from May to October [25,26]. The mean annual temperature ranges between approximately 12 and 18 °C, with seasonal variations typically spanning from minimum values near 5 °C during dry season (winter) nights to maximum values of around 28–30 °C during wet season (spring and summer). Annual precipitation ranges between 600 and 1000 mm, with approximately 70–80% of total rainfall occurring during the wet season [27].

The geological framework of Mexico City is controlled by the evolution of the Mexico Basin within the Trans-Mexican Volcanic Belt, a continental volcanic arc formed by the subduction of the Cocos and Rivera plates beneath the North American plate [28]. The basin is surrounded by volcanic ranges of predominantly andesitic to dacitic composition and contains a complex sequence of volcanic rocks, pyroclastic deposits, volcaniclastic materials, and lacustrine sediments associated with the former Lake Texcoco system. Consequently, soils in Mexico City range from volcanic-derived soils in elevated areas to clay-rich lacustrine soils in the central basin, characterized by high water retention and metal adsorption

capacity [29]. These geological and pedological conditions control the natural background levels of PTEs and influence the physicochemical properties of urban dust.

Land use within the city is heterogeneous, with highly urbanized zones concentrated in the central and northern sectors, while the southern and western areas include rural and semi-natural environments associated with mountainous terrains [30]. These contrasts in land use, together with climatic variability, influence the spatial distribution and seasonal dynamics of road dust and associated PTEs.

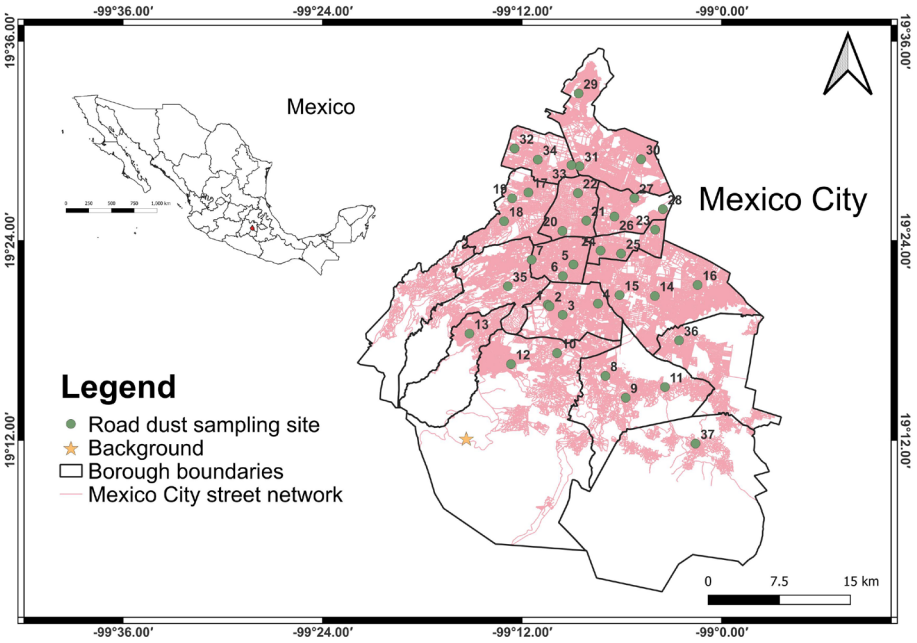


Figure 1. Location of the study area and sampling sites in Mexico City, Mexico.

2.2. Sampling and Chemical Analysis

Urban road dust sampling was conducted during two contrasting seasonal periods in Mexico City: the wet season (October 2021) and the dry season (March 2022). A total of 37 samples were collected during each campaign, resulting in 74 urban dust samples (Figure 1). In addition, two background samples, one for each season, were collected in a mountainous area located outside the urban footprint, selected to represent natural conditions with minimal anthropogenic influence. The sampling design aimed to achieve broad spatial coverage across Mexico City, including all administrative boroughs. Sampling locations were selected following a predefined strategy focused on areas with high vehicular activity, such as major avenues, primary roads, and heavily trafficked intersections. Site selection was also influenced by accessibility and safety conditions. At each location, surface road dust was collected directly from paved areas using a clean plastic scoop. Approximately 500 g of material was obtained per sample after removing coarse debris such as large particles. The collected material represents recently deposited and resuspended dust, which is more relevant for human exposure. Samples were stored in labeled polyethylene bags, and georeferenced using a GPS device.

Prior to chemical analysis, road dust samples were air-dried, homogenized, and sieved to obtain the <20 μm (635-mesh) fraction. This fine fraction was selected due to its higher surface area and greater potential for metal enrichment and interaction with biological systems. The concentrations of PTEs, including V, Cr, Mn, Co, Ni, Cu, As, Cd, Sb, and Pb, were determined using inductively coupled plasma–mass spectrometry (ICP–MS; iCAP Qc, Thermo Fisher Scientific, Waltham, MA, USA) at the Institute of Geophysics, National Autonomous University of Mexico (IGF-UNAM). Approximately 0.5 g of each

homogenized sample was subjected to total acid digestion using a mixture of concentrated HNO_3, HCl, and HF (9:3:2 mL) in Teflon vessels [31]. Digestion was carried out using a microwave-assisted system (ETHOS ONE, Milestone, Bergamo, Italy) equipped with a PRO-24 rotor to ensure complete dissolution of silicate and oxide phases [32]. After digestion, the solutions were evaporated to near dryness and subsequently re-dissolved in 50 mL of 3% ultrapure HNO_3 prior to ICP–MS analysis. Instrument calibration was performed using a multi-element standard curve (0–500 μg L^{-1}; ICP-MS-68A, High-Purity Standards, Charleston, SC, USA). Analytical accuracy was evaluated using the certified reference material NIST SRM 1648a (urban particulate matter), which was processed under the same conditions as the samples. Recovery rates for the analyzed elements were within ±10% of the certified values, except for As, which showed a recovery within ±15%. In addition, procedural blanks and replicate analyses were included to ensure data quality and analytical precision. Average recoveries (Table S1) for each element were: 100% (V), 94% (Cr), 102% (Mn), 96% (Co), 97% (Ni), 94% (Cu), 85% (As), 96% (Cd), 97% (Sb), and 99% (Pb). The detection limits (LD) for the analyzed elements, expressed in μg L^{-1}, were: V = 0.0037, Cr = 0.0003, Mn = 0.0085, Co = 0.0007, Ni = 0.0063, Cu = 0.0421, As = 0.0110, Cd = 0.0069, Sb = 0.0024, and Pb = 0.0129.

The selected PTEs represent elements commonly associated with both geogenic and anthropogenic sources in urban environments. V, Cr, Mn, Co, and Ni are typically linked to natural geological materials, whereas Cu, Sb, and Pb are recognized tracers of traffic-related emissions; As and Cd were included because of their toxicological relevance.

2.3. Geochemical Indices

To evaluate the degree of contamination and the potential ecological risk associated with PTEs in urban road dust, three geochemical indices were applied: the contamination factor (CF), the geoaccumulation index (Igeo), and the ecological risk index (RI). These indices provide complementary information regarding element enrichment relative to background conditions and their potential environmental impact [33,34]. In this study, C_b corresponds to the local background concentration obtained from road dust collected in a mountainous area outside the urbanized zone of Mexico City and minimally affected by anthropogenic activities. This local background was used in the calculation of CF, Igeo, and Er.

2.3.1. Contamination Factor

The CF was calculated to assess the degree of enrichment of each PTE relative to its background concentration [35]:

$$CF = \frac{C_n}{C_b} \quad (1)$$

where C_n is the concentration of the element in the sample. CF values were classified as follows: CF < 1 (low contamination), 1 ≤ CF < 3 (moderate contamination), 3 ≤ CF < 6 (considerable contamination), and CF ≥ 6 (very high contamination).

2.3.2. Geoaccumulation Index

The Igeo, originally proposed by Müller [36], was used to evaluate the degree of contamination:

$$Igeo = log_2\left(\frac{C_n}{1.5 \times C_b}\right) \quad (2)$$

where the constant 1.5 accounts for natural variability due to lithogenic effects. Igeo values were classified into seven categories: Igeo ≤ 0 (no contamination), 0 < Igeo ≤ 1 (low contamination), 1 < Igeo ≤ 2 (low to moderate contamination), 2 < Igeo ≤ 3 (moderate to

heavy contamination), 3 < Igeo ≤ 4 (heavy contamination), 4 < Igeo ≤ 5 (heavy to extreme contamination), and Igeo > 5 (extreme contamination).

2.3.3. Ecological Risk Index

The potential ecological risk factor (Er) for each element was calculated following Lv et al. [37]:

$$E_r = T_r \times CF \quad (3)$$

where T_r is the toxic response factor and CF is the contamination factor. The toxic response factors used in this study were: V = 2, Cr = 2, Mn = 1, Co = 5, Ni = 5, Cu = 5, As = 10, Cd = 30, Sb = 5, and Pb = 5. The classification of the individual Er is as follows: Er < 40 (low risk), 40 ≤ Er < 80 (moderate risk), 80 ≤ Er < 160 (considerable risk), 160 ≤ Er < 320 (high risk), and Er ≥ 320 (very high risk).

2.4. Spatial Analysis

Spatial distribution maps of PTEs in urban road dust were generated using a geographic information system (QGIS, version 3.34). Sampling locations were georeferenced in the field using a handheld GPS and recorded in the WGS 84 coordinate system (EPSG:4326). The analytical data were integrated with the spatial dataset to enable geochemical mapping [32]. Concentrations at each sampling site were represented using graduated symbols, with symbol size and color scaled according to the measured concentration of each element. Therefore, the maps show the spatial distribution of observed concentrations at the sampled locations rather than interpolated or predicted concentration surfaces. The maps were used as qualitative visualization tools to identify areas with relatively elevated measured concentrations and recurring spatial patterns between seasons [38]. They were overlaid on satellite imagery to provide geographic context and to facilitate the interpretation of spatial patterns in relation to urban infrastructure and land use. This approach supports the qualitative evaluation of potential emission sources while avoiding overinterpretation of unsampled areas [39].

2.5. Particle Characterization (SEM-EDS)

The morphology, particle size distribution, and semi-quantitative chemical composition of urban road dust were analyzed using a scanning electron microscope (SEM; Thermo Fisher Scientific Phenom Pro/ProX, Waltham, MA, USA). The analyses were performed on the <20 μm fraction due to its higher potential for resuspension and inhalation.

To ensure a representative dispersion of fine particles, samples were prepared using a resuspension chamber [6]. Sieved dust was placed in a polyethylene container, and a sampling holder was positioned at its center. A controlled flow of compressed air was applied to resuspend the material, allowing fine particles to settle onto the holder by gravity. This procedure promotes a more uniform particle distribution and facilitates the analysis of the respirable fraction. The preparation was conducted in triplicate to ensure reproducibility. Particle size distribution and morphological parameters were obtained from representative SEM images using Particle Metric Software (PMS) (https://www.thermofisher.com/mx/es/home/electron-microscopy/products/software-em-3d-vis/particle-software.html, accessed on 14 March 2026). The analyzed parameters included particle size (expressed as equivalent diameter) and circularity, enabling the characterization of particle shape and variability [31].

Samples were coated with a thin carbon layer to improve conductivity prior to imaging. Backscattered electron (BSE) images were acquired at an accelerating voltage of 15 kV to enhance compositional contrast. Energy-dispersive X-ray spectroscopy (EDS) was

performed in spot mode to obtain semi-quantitative elemental compositions of individual particles, allowing the identification of both mineral and anthropogenic components [40].

2.6. In Vitro Lung Bioaccessibility Test

Lung bioaccessibility was evaluated using an artificial lung fluid (ALF) extraction procedure, which simulates the acidic conditions of the phagolysosomal environment in alveolar macrophages (intracellular conditions). The ALF solution was prepared following a widely adopted formulation [41,42], and its chemical composition is provided in Table S2. The pH of the ALF solution was approximately 4.5.

A total of 30 samples were selected for bioaccessibility analysis, including 15 from the dry season and 15 from the wet season. The selection was based on both PTE concentrations and spatial distribution, in order to capture the variability across Mexico City. All experiments were performed on the <20 μm fraction, representing the respirable component of urban road dust. The extraction procedure involved mixing 0.01 g of sample with 10 mL of ALF solution in sterile tubes, corresponding to a solid-to-liquid (S/L) ratio of 1:1000. The suspensions were incubated at 37 °C for 24 h under controlled conditions with intermittent agitation to simulate pulmonary conditions. After incubation, the extracts were filtered through a 0.2 μm membrane and stored at 4 °C until analysis [6,22]. The concentrations of PTEs in the ALF extracts were determined by inductively coupled plasma–mass spectrometry (ICP–MS; Agilent 8800, Agilent Technologies Co., Ltd., Santa Clara, CA, USA) at the Laboratorio de Análisis de Elementos Traza, part of the Sistema de Laboratorios Especializados, Ciencias de la Tierra (SLE-CT) at Centro de Investigación Científica y de Educación Superior de Ensenada, Baja California (CICESE), Ensenada, Mexico. The bioaccessible fraction (%bio) of each element was calculated as a percentage of the total concentration using the following equation [6]:

$$\%bio = \frac{C_{bio} \times V}{C_{total} \times m} \quad (4)$$

where C_{bio} is the concentration of the element in the ALF extract (mg L^{-1}), V is the volume of the extraction solution (L), C_{total} is the total concentration of the element in the sample (mg kg^{-1}), and m is the mass of the sample (kg).

Instrument calibration was performed using 17-point standard curves prepared from certified reference solutions in 2% ultrapure HNO_3. An internal standard solution containing ^{103}Rh, ^{115}In, and ^{209}Bi was used to monitor signal stability during analysis. All measurements were performed in 5 replicates, and concentrations were averaged. Relative standard deviations (RSD) generally below 10%, indicating good analytical precision. Analytical recovery was evaluated by analyzing the SPS-SW1 certified reference materials and three ALF blank solutions spiked with a certified standard solution at concentrations of 5, 10 and 27 ppb. Recoveries for SPS-SW1 ranged between 98.3 and 114%, while those for the spiked ALF blank solutions ranged between 95.4 and 105.5%. In a small number of cases, calculated bioaccessibility values slightly exceeded 100%, which is attributable to the combined analytical uncertainty associated with total and dissolved concentration measurements. Consistent with previous bioaccessibility studies [17,31], values exceeding 100% were truncated to 100%.

2.7. Health Risk Assessment

The non-carcinogenic and carcinogenic health risks associated with exposure to PTEs in urban road dust were evaluated following the methodology proposed by the United States Environmental Protection Agency (USEPA) [43,44]. The assessment considered three

main exposure pathways: ingestion, inhalation, and dermal contact, for both children and adults.

The average daily dose (ADD) for each exposure pathway, ingestion (ADD_{ing}), inhalation (ADD_{inh}), and dermal contact (ADD_{der}), was calculated using the standard USEPA equations:

$$ADD_{ing} = \frac{C \times IngR \times EF \times ED}{BW \times AT} \times 10^{-6} \quad (5)$$

$$ADD_{inh} = \frac{C \times InhR \times EF \times ED}{PEF \times BW \times AT} \quad (6)$$

$$ADD_{der} = \frac{C \times SA \times AF \times ABF \times EF \times ED}{BW \times AT} \times 10^{-6} \quad (7)$$

Detailed information regarding the parameters, units, and exposure factors used in these calculations is provided in Table S3.

2.7.1. Non-Carcinogenic Risk

The potential non-carcinogenic risk was evaluated using the hazard quotient (HQ) and hazard index (HI). The HQ for each element and exposure pathway was calculated as:

$$HQ = \frac{ADD_i}{RfD_i} \quad (8)$$

where *RfD* (mg kg^{-1} day^{-1}) is the reference dose specific to each element and exposure route (Table S4). The hazard index (HI), representing the total non-carcinogenic risk, was obtained by summing the HQ values for all pathways and elements:

$$HI = \sum HQ_i \quad (9)$$

An HI value lower than 1 indicates no significant non-carcinogenic risk, whereas values equal to or greater than 1 suggest the potential for adverse health effects.

In addition to the conventional risk assessment based on total PTE concentrations, an inhalation-specific risk (HQ_{inh}) scenario was calculated using ALF-bioaccessible concentrations. For this purpose, the bioaccessible concentration of each element was obtained by multiplying the total concentration by its corresponding bioaccessibility percentage. The resulting concentrations were then incorporated into the standard USEPA inhalation exposure equations to estimate bioaccessibility-adjusted hazard quotients ($HQ_{inh\text{-}adj}$). This complementary approach provides a refined estimate of potential pulmonary exposure by considering only the fraction of each element that may become available under simulated lung-fluid conditions.

2.7.2. Carcinogenic Risk

Carcinogenic risk (CR) was estimated for elements classified as carcinogenic, including As, Cr, Ni, and Pb, based on their classification by the International Agency for Research on Cancer (IARC). The CR for each exposure pathway was calculated as:

$$CR = ADD_i \times SF \quad (10)$$

where *SF* is the carcinogenic slope factor for each element and exposure pathway [45,46]. The total carcinogenic risk (TCR) was obtained as the sum of individual risks:

$$TCR = \sum CR \quad (11)$$

According to USEPA guidelines, TCR values lower than 1×10^{-6} are considered negligible, values between 1×10^{-6} and 1×10^{-4} are regarded as acceptable, and values higher than 1×10^{-4} indicate an unacceptable carcinogenic risk.

2.8. Statistical Analysis

Descriptive statistical analysis was performed to summarize the concentrations of PTEs in urban road dust for both sampling seasons. Basic statistical parameters, including mean, median, standard deviation, minimum, and maximum values, were calculated for each element. To evaluate relationships among PTEs and identify potential common sources, Pearson correlation analysis was applied. The statistical significance of the correlations was assessed at a confidence level of 95% ($p < 0.05$) and 99% ($p < 0.01$). A correlation matrix was used to visualize the relationships among elements and to support the identification of potential common sources. Furthermore, multivariate statistical analysis was conducted using principal component analysis (PCA) to explore associations among elements and to identify potential source contributions. Prior to PCA, the dataset was standardized to eliminate the effect of differences in magnitude among variables. Components with eigenvalues greater than 1 were retained, and the results were interpreted based on the loadings of each element. All statistical analyses were performed using Python 3.11 (pandas, NumPy, and scikit-learn libraries), and graphical representations were generated using Matplotlib v3.11.

3. Results and Discussion

3.1. Seasonal Variability and Concentration Patterns of PTEs in Road Dust

Descriptive statistics for PTEs in road dust from Mexico City are presented in Table 1, while their seasonal distribution across sampling sites is shown in Figure 2. The mean concentrations in the dry season followed the order Mn > Cr > Cu > Pb > V > Ni > Co > As > Sb > Cd, whereas in the wet season the order was Mn > Cr > Pb > V > Cu > Ni > Co > As > Sb > Cd. Thus, Mn was the element with the highest concentration in both seasons, with mean concentrations of 846.5 mg kg^{-1} in the dry season and 839.1 mg kg^{-1} in the wet season, followed by Cr (183.9 and 192.3 mg kg^{-1}, respectively), whereas Cd consistently showed the lowest concentrations (0.9 mg kg^{-1} in both seasons). Pb and V also exhibited relatively high mean values, particularly in the wet season, reaching 165.6 and 145.0 mg kg^{-1}, respectively.

Table 1. Descriptive statistics of potentially toxic element (PTE) concentrations (mg kg^{-1}) in road dust during the dry and wet seasons.

	V	Cr	Mn	Co	Ni	Cu	As	Cd	Sb	Pb
Dry season										
Mean	127.7	183.9	846.5	13	52	160.4	8.2	0.9	7.5	135
Median	119.8	176.6	822.8	12.7	53.1	131.9	5.1	0.7	6.5	116.1
Min	89.5	98.6	554.7	9.5	31.6	36.2	0.4	0.3	2.7	58.7
Max	215.1	411.7	1518.1	20.4	117.9	417.3	57.6	4.8	19.5	528.9
SD	26.9	64.4	184.3	2.7	15.7	87.6	9.9	0.8	3.6	83
Wet season										
Mean	145	192.3	839.1	15.7	54.2	137.2	12.2	0.9	6.3	165.6
Median	132.4	184.1	782.3	14	46.9	116	9.8	0.7	5.8	150.1
Min	107.2	115.8	615.6	10.2	31.1	54.3	0.04	0.3	2.1	46.5
Max	269.2	397.8	1658.1	36.9	145.8	456	141.9	3.9	20.1	668.2
SD	33.5	61.2	189.9	5.6	24.9	78.3	22.4	0.8	3.6	97.2

Table 1. *Cont.*

	V	Cr	Mn	Co	Ni	Cu	As	Cd	Sb	Pb
Total [1]	136.4	188.1	842.8	14.4	53.1	148.8	10.7	0.9	6.9	150.3
Local background [2]	128.2	221.6	1157.5	20.1	59.4	34.5	9.4	0.5	0.9	37
Mexican SQL [3]	78	280	-	-	1600	-	22	37	-	400
Canadian SQG [4]	-	64	-	-	45	63	12	22	-	70
Dutch STV [5]	-	100	-	9	35	36	29	0.8	3	85

[1] average between dry and wet season; [2] average background values between seasons; [3] Soil Quality Limit [47]; [4] Soil Quality Guidelines [48]; [5] Soil Target Value [49].

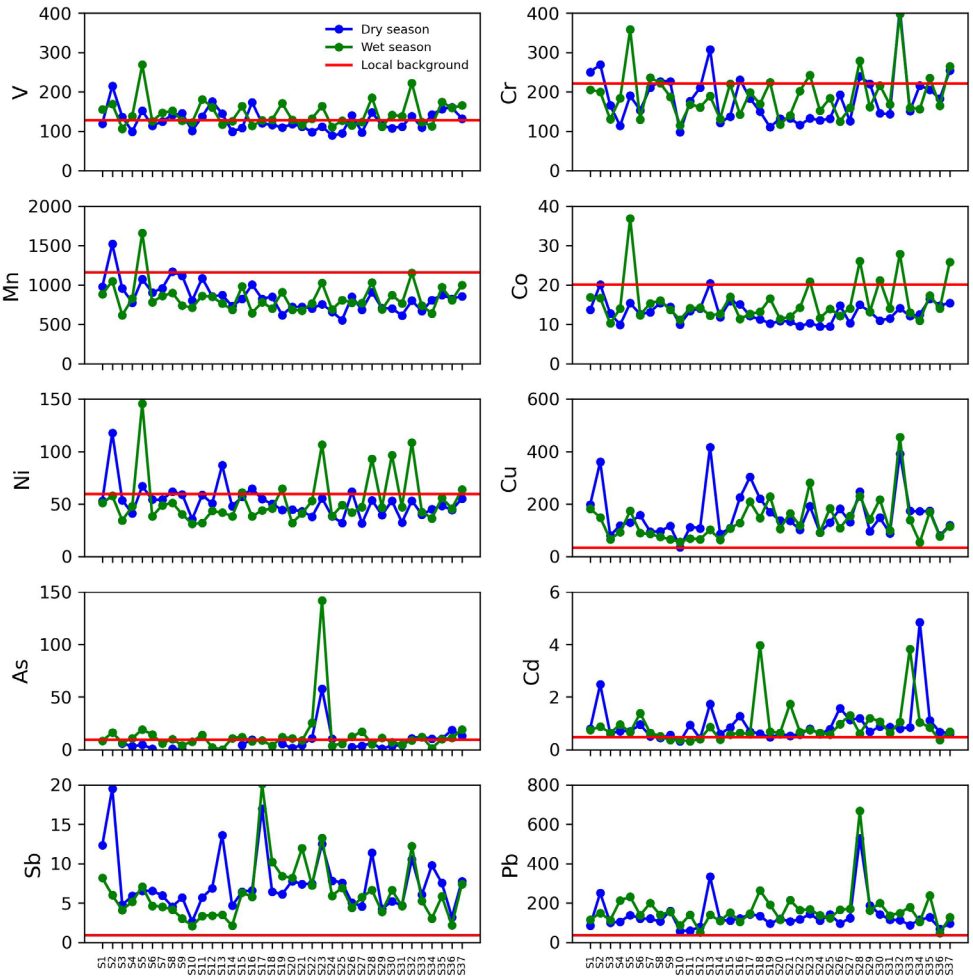


Figure 2. Concentrations (mg kg^{-1}) of PTEs in road dust samples collected during the dry and wet seasons across Mexico City. The red horizontal line indicates the local background value. Sampling sites are ordered according to site identification numbers (S1–S37).

A first relevant result is that seasonal contrasts were present, but not uniform across elements. Some PTEs showed slightly higher mean concentrations in the wet season, including V, Cr, Co, Ni, As, and Pb, while others, especially Cu, Sb, and Mn, were similar or slightly lower than in the dry season. This pattern suggests that seasonal effects in Mexico City road dust are not controlled by a single process. In many urban environments [46], rainfall is expected to reduce dust accumulation through washout and runoff, but this effect can be partially offset by local resuspension, redistribution of fine material, and continuous vehicular inputs [11]. In this dataset, the wet season does not simply reflect dilution or cleansing, but rather a dynamic redistribution of deposited particles across the urban surface. This interpretation is consistent with the site-by-site behavior shown in

Figure 2, where several elements display persistent hotspots in both seasons rather than a generalized seasonal decrease.

To determine whether seasonal differences were statistically significant, paired comparisons between dry- and wet-season concentrations were performed using the Wilcoxon signed-rank test (Table S5). This non-parametric approach was selected because several elements exhibited skewed distributions and localized concentration hotspots. The results revealed significant seasonal differences for V ($p = 0.012$), Co ($p = 0.014$), and Pb ($p = 0.008$), all showing higher concentrations during the wet season. In contrast, Cr, Mn, Ni, Cu, As, Cd, and Sb did not exhibit statistically significant differences between seasons ($p > 0.05$). These results indicate that spatial heterogeneity among sampling sites exerts a stronger control on PTE concentrations than seasonal variability for most elements. Therefore, although some differences in mean concentrations were observed between seasons, these changes were not statistically significant for the majority of the analyzed elements.

The largest concentration ranges were observed for Mn, Cr, Cu, As, and Pb. Mn varied from 554.7 to 1518.1 mg kg^{-1} in the dry season and from 615.6 to 1658.1 mg kg^{-1} in the wet season, indicating broad spatial variability despite similar seasonal means. Cr ranged from 98.6 to 411.7 mg kg^{-1} in the dry season and from 115.8 to 397.8 mg kg^{-1} in the wet season. Cu and Pb also showed pronounced variability, with maximum values of 417.3 and 528.9 mg kg^{-1} in the dry season, and 456.0 and 668.2 mg kg^{-1} in the wet season, respectively. Arsenic was especially heterogeneous in the wet season, reaching a maximum of 141.9 mg kg^{-1}, far above both its mean (12.2 mg kg^{-1}) and median (9.8 mg kg^{-1}), indicating the presence of localized anomalies. These wide ranges, together with the relatively high standard deviations reported in Table S6, point to a strong influence of local emission sources superimposed on the urban geochemical background. Comparison with the local background confirms that enrichment is widespread but element-specific. As illustrated in Figure 2 and summarized in Figure S1, Cu, Sb, and Pb stand out as the most consistently enriched elements. Cu, Sb, and Pb exceeded background concentrations at 100% of sampling sites during both the dry and wet seasons. Cd showed very high exceedance frequencies as well, affecting 89.2% of sites in the dry season and 83.8% in the wet season. In contrast, Mn displayed the lowest exceedance percentages, with only 5.4% of sites above background in the dry season and 2.7% in the wet season, which agrees with the boxplot pattern in Figure S2 where Mn concentrations are generally below the local background line despite being the most abundant element. This indicates that Mn is predominantly of geogenic origin and largely controlled by the natural geochemical framework of the basin, whereas Cu, Sb, Pb, and Cd are more strongly influenced by anthropogenic inputs.

When the observed concentrations are compared with regulatory and target values, several noteworthy patterns emerge (Table 1). Relative to the Mexican Soil Quality Limits [47], mean V concentrations in both seasons (127.7 and 145.0 mg kg^{-1}) were higher than the reference value of 78 mg kg^{-1}, whereas the remaining analyzed PTEs were below the corresponding Mexican criteria. In contrast, comparison with the Canadian Soil Quality Guidelines [48] indicates that mean concentrations of Cr, Ni, Cu, and Pb exceeded their respective guideline values during both seasons. Cr concentrations were approximately three times higher than the Canadian benchmark of 64 mg kg^{-1}, Cu exceeded the guideline value of 63 mg kg^{-1} by more than a factor of two, and Pb concentrations were approximately 1.9 and 2.4 times higher than the guideline value of 70 mg kg^{-1} during the dry and wet seasons, respectively. Mean Ni concentrations also exceeded the Canadian guideline value of 45 mg kg^{-1} in both seasons, whereas As remained below the Canadian benchmark during the dry season and was slightly above it during the wet season. Cd remained well below the Canadian guideline value. Comparison with the Dutch Soil Target Values [49]

reveals a similar pattern. Mean concentrations of Co, Cr, Ni, Cu, Sb, and Pb exceeded their respective target values in both seasons. Cu showed the largest exceedance relative to the Dutch target value of 36 mg kg^{-1}, while Sb exceeded its target value of 3 mg kg^{-1} by more than a factor of two. Pb concentrations also remained above the Dutch target value of 85 mg kg^{-1} in both seasons. Co concentrations exceeded the Dutch target value of 9 mg kg^{-1} by approximately 1.4–1.7 times, whereas Cr and Ni exceeded their respective target values of 100 and 35 mg kg^{-1}. Mean Cd concentrations were close to the Dutch target value of 0.8 mg kg^{-1}, while As remained below the Dutch target value of 29 mg kg^{-1} in both seasons. Because no regulatory thresholds currently exist for the <20 μm fraction of road dust, the concentrations measured in this study were compared with selected soil quality criteria and target values only as screening-level reference benchmarks. These comparisons should be interpreted cautiously because the analyzed material corresponds to a fine road-dust fraction that is typically enriched in PTEs relative to bulk soils.

These results show that road dust in Mexico City contains a complex mixture of geogenic and anthropogenic signatures. Mn, and to some extent Co, are closer to local background conditions and likely reflect the volcanic-lacustrine geochemical setting of the basin. In contrast, Cu, Sb, Pb, Cd, and part of the Ni and Cr burden are more consistent with diffuse urban emissions, especially traffic-related non-exhaust sources. The fact that Cu, Sb, and Pb exceeded the local background at all sampled sites underscores the pervasive impact of vehicular activity across the city. Therefore, even before applying geochemical indices or multivariate statistics, the descriptive results indicate that Mexico City road dust is widely enriched in several traffic-sensitive PTEs. Furthermore, the limited number of statistically significant seasonal differences suggests that spatial heterogeneity associated with urban activities exerts a stronger influence on PTE concentrations than seasonal variability. The observed seasonal differences likely reflect the combined effects of rainfall washout, particle redistribution, resuspension processes, and the continuous emission of traffic-related particles rather than simple dilution effects alone.

3.2. Geochemical Indices and Contamination Assessment

The degree of contamination in Mexico City road dust was further evaluated using the contamination factor (CF), geoaccumulation index (Igeo), and potential ecological risk factor (Er). Mean values for both seasons are summarized in Figure 3, whereas full descriptive statistics are presented in Table 2. Together, these indices provide complementary evidence regarding elemental enrichment, anthropogenic influence, and possible ecological implications.

The CF revealed marked differences among elements and confirmed that anthropogenic enrichment is concentrated in a limited group of PTEs. Mean CF values in the dry season followed the order Sb (8.1) > Cu (4.6) > Pb (3.6) > Cd (1.9) > V (1.0) > Ni (0.9) = As (0.9) > Cr (0.8) > Mn (0.7) > Co (0.6). A similar trend was observed in the wet season, with Sb (6.8) > Pb (4.5) > Cu (3.9) > Cd (1.9) > As (1.4) > V (1.1) > Ni (0.9) > Cr (0.9) > Co (0.8) > Mn (0.7). According to the CF classification, most elements, including Mn, Co, Cr, and Ni, indicated low contamination (CF < 1) during both the dry and wet seasons, suggesting a strong influence of natural background levels and limited anthropogenic enrichment. V exhibited CF values close to the threshold between low and moderate contamination, increasing from 1.0 in the dry season to 1.1 in the wet season. As showed a more pronounced seasonal change, increasing from 0.9 during the dry season (low contamination) to 1.4 during the wet season, thereby reaching the moderate contamination category. Cd consistently exhibited moderate contamination, with mean CF values of 1.9 in the dry season and 1.9 in the wet season. In contrast, Cu and Pb were classified as considerably contaminated in both seasons, with mean CF values of 4.6 and 3.6 during the dry season,

and 3.9 and 4.5 during the wet season, respectively. The highest CF values corresponded to Sb, which reached mean values of 8.1 in the dry season and 6.8 in the wet season, placing it in the category of very high contamination. This result strongly supports the use of Sb as a tracer of traffic-derived emissions, particularly brake wear, as reported in numerous urban dust studies [50,51]. The lower CF values observed for Cu and Sb during the wet season compared with the dry season may reflect the partial washout and redistribution of fine particles by rainfall. In contrast, the increases in Pb, As, and V from the dry season to the wet season suggest continued atmospheric deposition or remobilization from localized urban sources. These results indicate that seasonality modifies the magnitude of contamination but does not alter the dominant contamination profile of the city, which remains strongly influenced by Sb, Cu, Pb, and Cd.

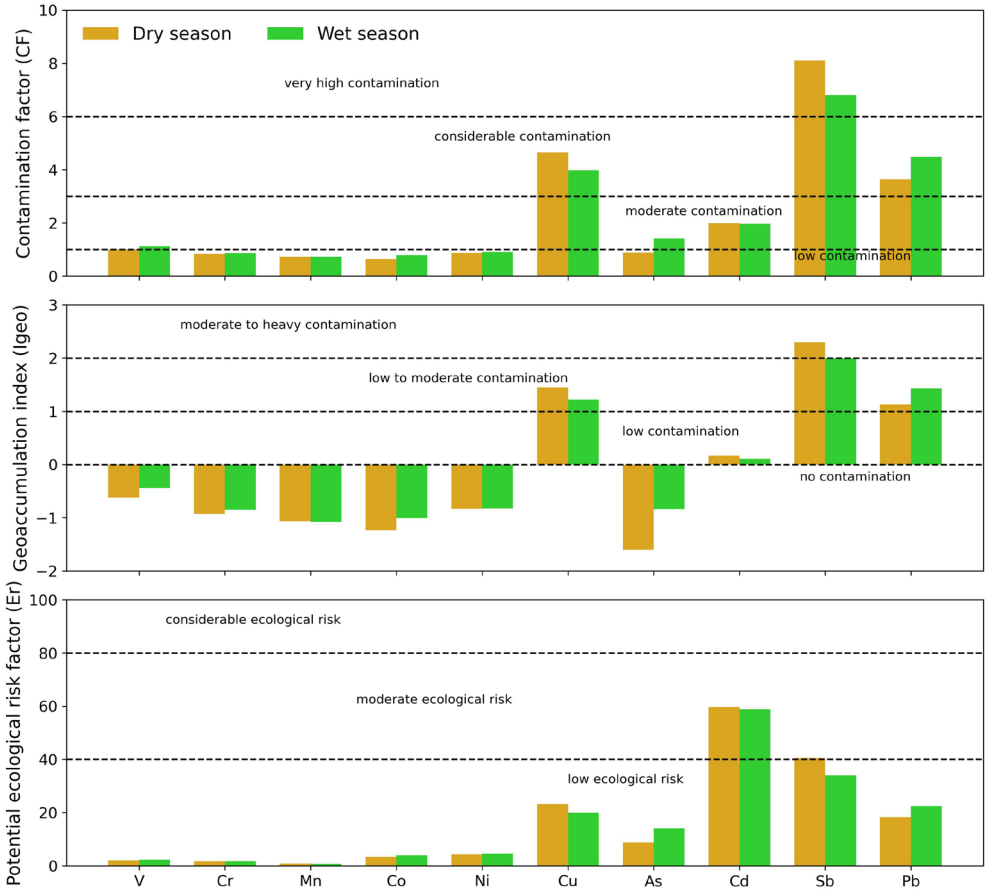


Figure 3. Seasonal comparison of PTEs in Mexico City road dust. Mean values of contamination factor (CF), geoaccumulation index (Igeo), and potential ecological risk factor (Er) are shown for the dry season (orange bars) and wet season (green bars). Dashed horizontal lines indicate classification thresholds commonly used to interpret contamination level and ecological risk categories.

The Igeo provided a more conservative estimate of anthropogenic influence because it incorporates a background correction factor. Mean Igeo values for Mn, Co, Cr, Ni, V, and As were negative during both the dry and wet seasons, indicating an uncontaminated status with respect to these elements. This pattern is consistent with the CF results and suggests that these elements are largely controlled by natural lithogenic inputs derived from the volcanic and lacustrine materials that dominate the Mexico Basin. In contrast, Cu, Pb, Cd, and especially Sb showed positive Igeo values in both seasons. Cu exhibited mean Igeo values of 1.4 during the dry season and 1.2 during the wet season, corresponding to a moderately contaminated status. Pb showed similar behavior, with mean Igeo values of 1.1 in the dry season and 1.4 in the wet season, also indicating moderate contamination. Cd

remained close to zero, with mean Igeo values of 0.2 during the dry season and 0.1 during the wet season, suggesting a transition between uncontaminated and slightly contaminated conditions. Sb again stood out as the most enriched element, reaching mean Igeo values of 2.3 in the dry season and 1.9 in the wet season. These values indicate moderate to heavy contamination during the dry season and moderate contamination during the wet season, reinforcing that Sb was the most anomalous element in the dataset. The agreement between CF and Igeo strongly indicates that Sb enrichment is widespread and persistent across seasons, despite the slight decrease observed during the wet season.

Table 2. Descriptive statistics of contamination factor (CF), geoaccumulation index (Igeo), and potential ecological risk factor (Er) during the dry and wet seasons.

	V	Cr	Mn	Co	Ni	Cu	As	Cd	Sb	Pb
Dry season										
CF										
Mean	1	0.8	0.7	0.6	0.9	4.6	0.9	1.9	8.1	3.6
Median	0.9	0.8	0.7	0.6	0.9	3.8	0.5	1.5	7	3.1
Min	0.7	0.4	0.5	0.5	0.6	1.0	0.1	0.7	2.9	1.6
Max	1.7	1.9	1.3	1	1.9	12.1	6.1	10.3	21	14.3
SD	0.2	0.3	0.2	0.1	0.3	2.5	1.2	1.7	3.9	2.2
Igeo										
Mean	−0.6	−0.9	−1.1	−1.2	−0.8	1.4	−1.6	0.2	2.3	1.1
Median	−0.7	−0.9	−1.1	−1.2	−0.7	1.3	−1.5	0	2.2	1.1
Min	−1.1	−1.7	−1.6	−1.7	−1.5	−0.6	−5.2	−1.2	0.9	−0.1
Max	0.2	0.3	−0.2	−0.6	0.4	3	2	2.8	3.8	3.2
SD	0.3	0.5	0.3	0.3	0.4	0.7	1.7	0.7	0.6	0.6
Er										
Mean	1.9	1.7	0.7	3.2	4.4	23.3	8.8	59.7	40.5	18.2
Median	1.9	1.6	0.7	3.2	4.5	19.1	5.4	44.7	35.2	15.7
Min	1.4	0.9	0.5	2.3	2.7	5.1	0.4	19.8	14.3	7.9
Max	3.3	3.7	1.3	5.1	9.9	60.5	61.5	309.6	105.1	71.5
SD	0.4	0.6	0.2	0.7	1.3	12.7	11.8	49.8	19.5	11.2
Wet season										
CF										
Mean	1.1	0.9	0.7	0.8	0.9	3.9	1.4	1.9	6.8	4.5
Median	1	0.8	0.7	0.7	0.8	3.4	1	1.4	6.2	4.1
Min	0.8	0.5	0.5	0.5	0.5	1.6	0.0	0.7	2.3	1.3
Max	2.1	1.8	1.4	1.8	2.4	13.2	15.2	8.4	21.6	18.1
SD	0.3	0.3	0.2	0.3	0.4	2.3	2.4	1.7	3.9	2.6
Igeo										
Mean	−0.4	−0.8	−1.1	−1	−0.8	1.2	−0.8	0.1	1.9	1.4
Median	−0.5	−0.8	−1.1	−1.1	−0.9	1.2	−0.5	−0.1	2	1.4
Min	−0.8	−1.5	−1.5	−1.6	−1.5	0.1	−8.5	−1.1	0.6	−0.3
Max	0.5	0.3	−0.1	0.3	0.7	3.1	3.3	2.5	3.8	3.6
SD	0.3	0.4	0.3	0.4	0.5	0.7	1.7	0.8	0.7	0.6
Er										
Mean	2.3	1.7	0.7	3.9	4.6	19.9	14.1	58.8	34	22.4
Median	2.1	1.7	0.7	3.5	3.9	16.8	10.5	42.8	31.1	20.3
Min	1.7	1	0.5	2.5	2.6	7.9	0.1	20.4	11.3	6.3
Max	4.2	3.6	1.4	9.2	12.3	66.1	151.7	253.4	108.1	90.3
SD	0.5	0.5	0.2	1.4	2.1	11.3	23.9	50.1	19.3	13.1

The Er integrates contamination level with toxic-response coefficients, thereby emphasizing elements of higher environmental concern. Mean Er values were generally low for V, Cr, Mn, Co, Ni, and As during both the dry and wet seasons, all remaining well below the threshold of 40. Cu also remained within the low ecological risk category despite its elevated concentrations, with mean Er values of 23.3 during the dry season and 19.88 during the wet season. The highest ecological concern corresponded to Cd, which reached mean Er values of 59.7 in the dry season and 58.8 in the wet season, placing it within the moderate ecological risk category. Although Cd concentrations were relatively low in absolute terms, its high toxic-response coefficient strongly amplified its ecological significance. This demonstrates that concentration alone is insufficient to evaluate environmental relevance, since relatively low Cd levels may still pose disproportionate ecological concern. Sb represented the second most relevant element from the ecological perspective, with mean Er values of 40.5 during the dry season and 34 during the wet season. These values place Sb at the boundary between low and moderate ecological risk, particularly during the dry season. Pb also showed non-negligible ecological risk values, increasing from 18.2 in the dry season to 22.4 in the wet season, whereas As increased from 8.8 during the dry season to 14.1 during the wet season. Occasional maximum values were particularly notable, including Cd (309.6), As (151.7), and Sb (108.1), indicating localized hotspots where ecological risk may be substantially higher than the citywide mean.

The three indices consistently identify two contrasting elemental groups. The first group (Mn, Co, Cr, Ni, and partly V) is characterized by low CF values, negative Igeo values, and negligible ecological risk, suggesting a dominant geogenic origin related to regional soils and volcanic parent materials. The second group (Sb, Cu, Pb, Cd, and to a lesser extent As) displays anthropogenic enrichment and higher ecological relevance, reflecting urban emission sources. Among all analyzed elements, Sb exhibited the highest degree of contamination, with the highest CF and Igeo values in both seasons. Cu and Pb showed similar enrichment patterns, supporting a common traffic-related origin associated with non-exhaust emissions. Although less enriched, Cd dominated the ecological risk profile because of its high toxic-response coefficient. Overall, the indices indicate that road dust contamination in Mexico City is driven by a specific subset of traffic-sensitive PTEs rather than by generalized enrichment across all elements. Seasonal differences were observed mainly in contamination magnitude, whereas the persistent enrichment of Cu, Sb, Pb, and Cd suggests sustained urban emission sources. As showed more variable behavior, with moderate enrichment only during the wet season. It should be noted that CF, Igeo, and Er are influenced by the selected background concentrations. Although a local background was used to better represent natural conditions, the geological complexity of the Mexico Basin introduces some uncertainty into the calculated values. Therefore, these indices should be interpreted as screening-level indicators of enrichment and ecological risk rather than absolute measures of contamination. For this reason, interpretations were supported by spatial distribution patterns, correlation analysis, PCA, and SEM–EDS particle characterization.

3.3. Spatial Distribution of PTEs

The spatial distribution of PTEs in Mexico City road dust is presented in Figures 4 and 5 for both the dry and wet seasons. In general, the maps reveal pronounced spatial heterogeneity, with localized hotspots rather than uniform citywide gradients. This pattern is consistent with the strong site-to-site variability previously observed in the descriptive statistics and geochemical indices, indicating that local emission sources exert greater control than seasonal meteorological changes.

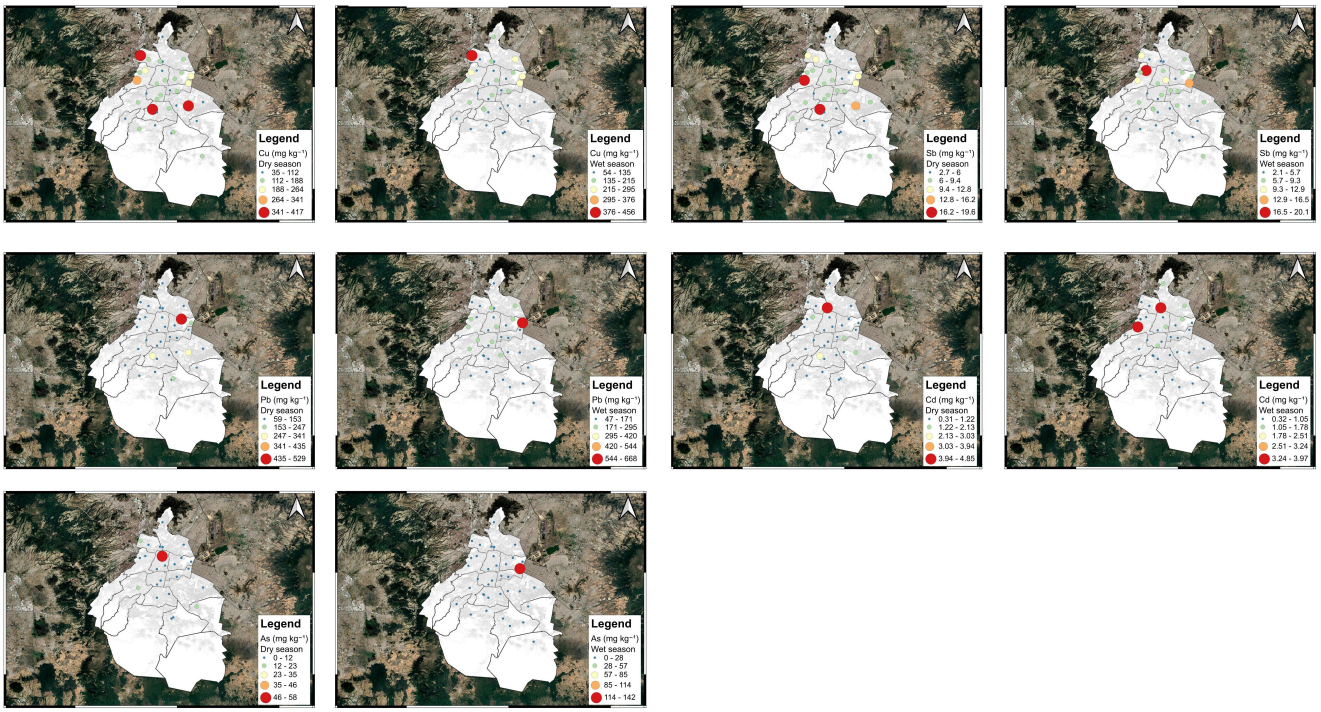


Figure 4. Spatial distribution of traffic-related PTEs in Mexico City road dust during the dry and wet seasons. Maps show concentrations of Cu, Sb, Pb, Cd, and As (mg kg^{-1}) at the 37 sampling sites. Color classes represent concentration intervals from lower (blue/green) to higher values (red), highlighting localized hotspots and seasonal differences in concentration magnitude.

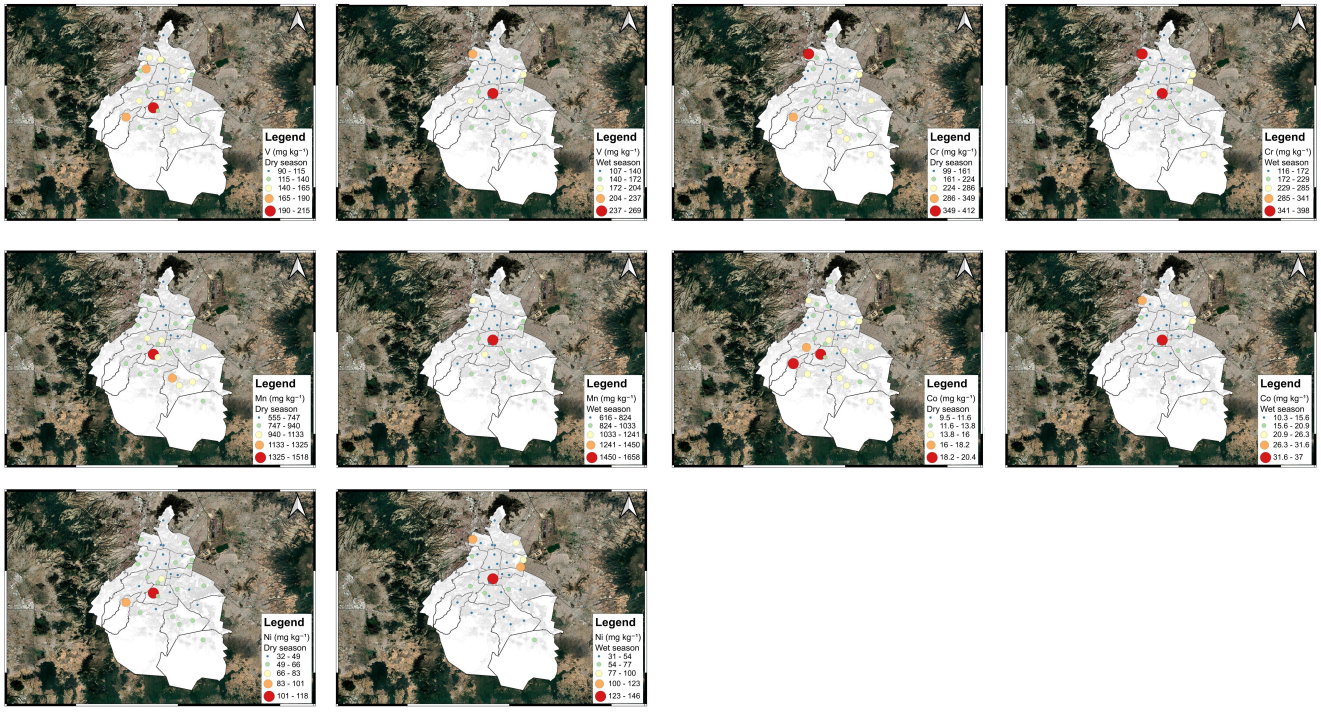


Figure 5. Spatial distribution of geogenic or mixed-source PTEs in Mexico City road dust during the dry and wet seasons. Maps show concentrations of V, Cr, Mn, Co, and Ni (mg kg^{-1}) at the sampling sites. Color gradients indicate increasing concentrations, allowing visualization of spatial variability and recurrent hotspots between seasons.

Figure 4 shows the distribution of Cu, Sb, Pb, Cd, and As, which were previously identified as the most enriched and environmentally relevant elements. Cu displayed multiple

hotspots in both seasons, mainly concentrated in the northern and central sectors of the city, with maximum values of 417.3 mg kg^{-1} in the dry season and 456 mg kg^{-1} in the wet season. The persistence of these hotspots across seasons suggests continuous local emissions rather than episodic inputs. However, comparison between seasons also shows that Cu concentrations decreased substantially during the wet season at three of the four sites with the highest concentrations, suggesting partial washout, redistribution of fine particles, or reduced accumulation under wetter conditions. Despite this decrease in intensity, the spatial recurrence of the main hotspots indicates that traffic-related Cu emissions remain persistent throughout the year. Given the strong enrichment of Cu indicated by CF and Igeo, these spatial patterns are consistent with traffic-related non-exhaust sources [52], particularly brake wear and vehicular abrasion [53]. Sb exhibited a similar but more localized pattern, with the highest values concentrated in northern and central sampling points. Maximum concentrations reached 19.6 mg kg^{-1} during the dry season and 20.1 mg kg^{-1} in the wet season. The spatial coincidence between Sb and Cu hotspots strongly suggests a common source, supporting the interpretation of brake wear emissions [50,54] as a dominant contributor. The persistence of elevated Sb concentrations during both seasons also indicates that rainfall does not substantially eliminate this contamination signal. Pb showed a highly focused distribution, with one major hotspot in the northeastern sector during both seasons, reaching 528.9 mg kg^{-1} in the dry season and 668.2 mg kg^{-1} in the wet season. Outside this hotspot, Pb concentrations were substantially lower but still elevated across many sites. This behavior suggests the coexistence of diffuse urban Pb contamination with localized legacy sources, such as historically contaminated dust deposits, industrial emissions, or intense traffic corridors [55,56] where previously deposited Pb-rich particles continue to be resuspended. Cd concentrations were generally low in absolute terms, but the maps reveal distinct hotspots in the northern-central area during both seasons, with maximum values close to 4–5 mg kg^{-1}. This is relevant because Cd showed the highest ecological risk factor despite low concentrations, highlighting the importance of toxicity-weighted indices. As also displayed discrete hotspots rather than broad enrichment, with the most pronounced anomaly in the wet season reaching 142 mg kg^{-1}. Such isolated peaks may indicate localized industrial, commercial, or combustion-related sources [57], although some contribution from regional geogenic materials cannot be excluded.

Figure 5 presents the distribution of V, Cr, Mn, Co, and Ni, which generally exhibited lower enrichment factors and stronger background influence. Nevertheless, these elements also showed identifiable hotspots, indicating that natural control does not exclude additional urban contributions. V displayed elevated concentrations mainly in northern and northwestern sectors during both seasons, with maxima of 215.1 mg kg^{-1} (dry) and 269.2 mg kg^{-1} (wet). This distribution may reflect mixed inputs from crustal materials and combustion-related emissions, since V is commonly associated with fuel oil combustion and thermoelectric power plant emissions [58,59], but can also occur in volcanic-derived parent materials. Cr showed a repeated pattern of northern-central hotspots in both seasons, with maximum concentrations of 411.7 and 397.8 mg kg^{-1}, respectively. Although Cr did not show strong enrichment relative to background in the CF analysis, these localized high values suggest additional anthropogenic inputs superimposed on natural concentrations. Potential sources include traffic abrasion, industrial activities, and construction-related materials [52,60]. Mn, the most abundant element in the dataset, exhibited a relatively widespread distribution with fewer extreme hotspots than Cu or Pb. Concentrations remained high across much of the city, with maxima of 1518.1 mg kg^{-1} in the dry season and 1658.1 mg kg^{-1} in the wet season. However, because Mn values were generally close to the local background, its spatial pattern likely reflects the natural geochemical composition of soils and volcanic-lacustrine sediments, with only minor anthropogenic enhancement. Co

and Ni displayed similar spatial behavior, with scattered moderate anomalies and recurrent hotspots in central to northern sectors. Maximum Co values reached 20.4 mg kg^{-1} in the dry season and 37 mg kg^{-1} in the wet season, whereas Ni reached 117.8 and 145.8 mg kg^{-1}, respectively. Their co-occurrence may indicate mixed sources including crustal particles, traffic wear, and industrial inputs [19].

A notable feature of Figures 4 and 5 is that the main hotspots remained broadly consistent between the dry and wet seasons, although their intensity varied. This persistence suggests stable emission sources, while seasonal differences likely reflect meteorological influences such as rainfall-driven redistribution and removal of deposited particles. Most hotspots were concentrated in the northern, northeastern, and central sectors of the city, areas characterized by dense urbanization, intense traffic activity, commercial development, and historical industrial influence. In contrast, southern sectors generally exhibited lower PTE concentrations, consistent with lower traffic density and greater proximity to semi-natural areas. Previous studies [61,62] have shown that emissions originating from the northern Metropolitan Zone can affect large portions of Mexico City, potentially contributing to the elevated PTE concentrations observed in this sector. The spatial patterns indicate that road dust contamination is strongly heterogeneous and closely linked to urban land use. Traffic-sensitive elements such as Cu, Sb, and Pb exhibited the most pronounced hotspot patterns, whereas Mn and part of the V–Cr–Ni group retained a stronger geogenic signature.

3.4. Source Identification of PTEs

The Pearson correlation matrix (Table 3) revealed two major association groups that were broadly consistent between the dry and wet seasons.

Table 3. Pearson correlation coefficients (r) of PTEs in road dust from Mexico City during the dry and wet season.

	V	Cr	Mn	Co	Ni	Cu	As	Cd	Sb	Pb
Dry season										
V	1.00	0.63 **	0.76 **	0.80 **	0.73 **	0.48 **	0.07	0.34 *	0.47 **	0.41 *
Cr		1.00	0.48 **	0.72 **	0.54 **	0.57 **	−0.03	0.28	0.54 **	0.38 *
Mn			1.00	0.70 **	0.82 **	0.36 *	0.14	0.21	0.41 *	0.29
Co				1.00	0.81 **	0.42 *	0.02	0.26	0.45 **	0.37 *
Ni					1.00	0.39 *	0.11	0.18	0.36 *	0.24
Cu						1.00	0.19	0.62 **	0.74 **	0.69 **
As							1.00	0.15	0.11	0.18
Cd								1.00	0.58 **	0.55 **
Sb									1.00	0.72 **
Pb										1.00
Wet season										
V	1.00	0.79 **	0.76 **	0.83 **	0.80 **	0.63 **	0.28	0.32	0.51 **	0.49 **
Cr		1.00	0.67 **	0.78 **	0.71 **	0.58 **	0.19	0.27	0.46 **	0.44 **
Mn			1.00	0.73 **	0.84 **	0.41 *	0.12	0.21	0.38 *	0.29
Co				1.00	0.85 **	0.46 **	0.22	0.31	0.49 **	0.40 *
Ni					1.00	0.43 *	0.18	0.24	0.41 *	0.35 *
Cu						1.00	0.35 *	0.66 **	0.71 **	0.74 **
As							1.00	0.29	0.34 *	0.39 *
Cd								1.00	0.55 **	0.58 **
Sb									1.00	0.77 **
Pb										1.00

**: Correlation is significant at the 0.01 level (two-tailed). *: Correlation is significant at the 0.05 level (two-tailed).

The first group included V, Cr, Mn, Co, and Ni, which showed strong and statistically significant positive correlations (generally r = 0.63–0.85, $p < 0.01$). For example, in the dry season, V correlated strongly with Co (r = 0.80), Mn (r = 0.76), and Ni (r = 0.73), while Mn and Ni were also highly associated (r = 0.82). Similar or stronger relationships were observed during the wet season, including Co–Ni (r = 0.85), Mn–Ni (r = 0.84), and V–Co (r = 0.83). These consistent associations suggest a common lithogenic or crustal origin, likely linked to the volcanic and lacustrine parent materials that characterize the Mexico Basin. Resuspension of local soils and road sediments likely contributes to the presence of this elemental group in urban dust. A second association group was defined by Cu, Sb, Pb, and Cd. Cu showed strong positive correlations with Sb (r = 0.74 dry; 0.71 wet), Pb (r = 0.69 dry; 0.74 wet), and Cd (r = 0.62 dry; 0.66 wet). Sb was also highly correlated with Pb (r = 0.72 dry; 0.77 wet) and Cd (r = 0.58 dry; 0.55 wet). These relationships strongly indicate common anthropogenic sources and are characteristic of non-exhaust vehicular emissions. In particular, Sb is widely recognized as a tracer of brake pad abrasion, whereas Cu is commonly associated with brake components and mechanical wear [63]. Pb, although phased out from gasoline, remains persistent in urban environments through legacy deposits, brake materials, tire wear, and the continual resuspension of historically contaminated particles [64]. Cd may derive from tire wear, lubricants, industrial residues, and mixed traffic-related sources [65]. As displayed the weakest correlations with most other PTEs in both seasons, suggesting a more complex or independent origin. In the dry season, As was largely uncorrelated with the remaining elements, whereas in the wet season modest correlations emerged with Cu (r = 0.35), Sb (r = 0.34), and Pb (r = 0.39). This behavior may reflect localized point sources, combustion-related emissions, or mixed anthropogenic inputs superimposed on variable natural background concentrations.

The PCA results (Figures 6 and S3) further supported these interpretations. The first two principal components explained 64.9% of the total variance, with PC1 accounting for 49.6% and PC2 for 15.3%. PC1 was dominated by positive loadings of most elements, especially Cr, Ni, Mn, Co, and V, together with contributions from Cu, Sb, and Pb. This component likely represents the integrated urban dust matrix, combining resuspended crustal materials with widespread anthropogenic deposition. In contrast, PC2 was strongly influenced by Cd, Sb, Cu, and Pb, suggesting a traffic-related factor consistent with brake wear and other vehicular non-exhaust processes. The upward orientation of these vectors in the biplot distinguishes them from the more geogenic V–Mn–Co–Ni group, which plotted toward lower PC2 values. The score distribution also suggests partial seasonal separation. Several wet-season samples were displaced toward positive PC1 values, reflecting sites with elevated concentrations of traffic-sensitive metals such as Cu, Sb, and Pb. Meanwhile, many dry-season samples clustered closer to the central region of the biplot, although overlap between seasons remained substantial. This suggests that seasonal conditions primarily influence concentration levels and spatial redistribution, whereas the geogenic and traffic-related factor structure remains broadly stable throughout the year.

The Cu–Sb relationship shown in Figure 7 provides particularly strong evidence for a traffic-related source, including vehicular brake wear, as an important contributor to PTEs in Mexico City road dust. Cu and Sb exhibited a robust positive correlation (r = 0.74; $R^2 = 0.55$), supporting their co-occurrence across multiple sampling sites and seasons. Because both elements are common constituents of brake pads, their coupled enrichment is widely recognized as an indicator of non-exhaust traffic emissions. In addition, the inclusion of the local background and upper continental crust [66] values in Figure 7A highlights that nearly all urban samples are strongly shifted toward higher Cu and Sb concentrations relative to natural reference materials, reinforcing the predominance of anthropogenic enrichment. The Cu/Sb ratio varied spatially, generally ranging from approximately 10

to 37, with broadly comparable patterns between dry and wet seasons (Figure 7B). Such variability likely reflects differences in traffic intensity, braking frequency, fleet composition, vehicle age, and the contribution of additional Cu-bearing sources. Previous studies have shown that Cu/Sb ratios are effective tracers of vehicular abrasion processes, particularly brake wear, with reported values commonly ranging from ~2 to 13 in road dust, urban PM, and brake abrasion particles [67–70]. Das et al. [63], for example, reported Cu/Sb ratios of approximately 8 for urban $PM_{2.5}$ and summarized similar ratios associated with traffic-derived particles, brake linings, and road dust. The generally elevated Cu/Sb ratios observed in this study therefore support a dominant contribution from traffic-related non-exhaust emissions, while the wider range observed at some sites may indicate mixing with additional Cu-rich urban sources. Nevertheless, the persistence of relatively consistent Cu–Sb relationships across the city indicates that traffic-derived brake abrasion likely represents one of the major contributors to road dust composition in Mexico City.

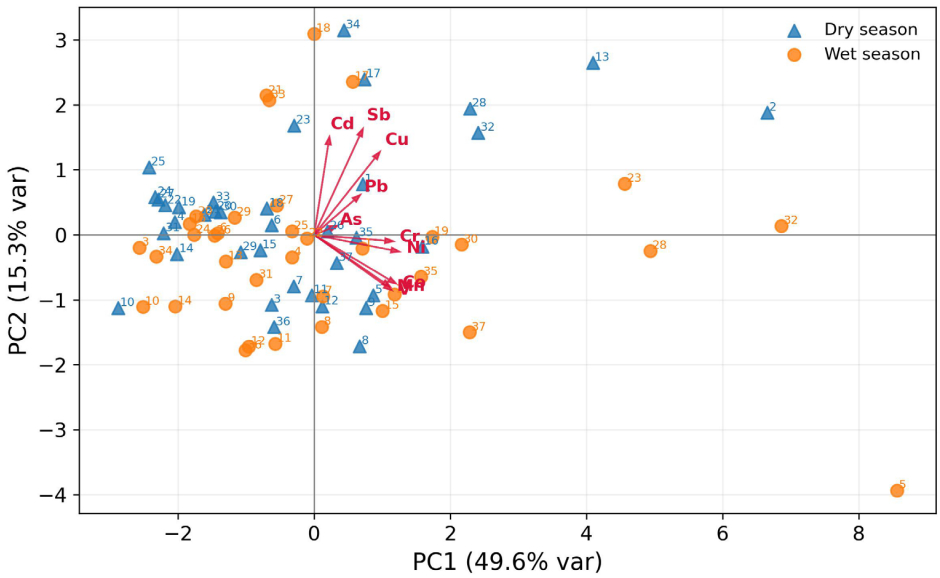


Figure 6. Principal component analysis (PCA) biplot of PTEs in Mexico City road dust considering both sampling seasons. Dry-season samples are shown as blue triangles and wet-season samples as orange circles. Red vectors represent elemental loadings on the first two principal components (PC1 and PC2), which explain 49.6% and 15.3% of the total variance, respectively.

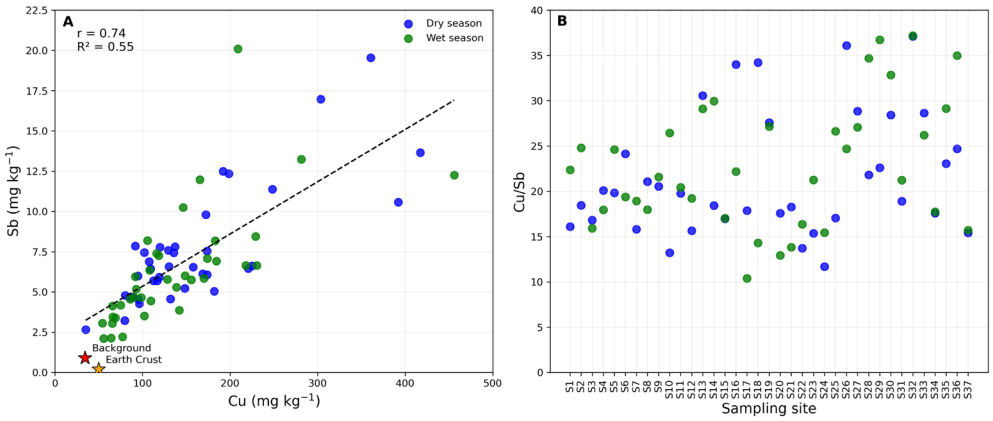


Figure 7. Relationships between Cu and Sb concentrations in Mexico City road dust. (**A**) Scatter plot of Sb versus Cu concentrations for dry-season (blue) and wet-season (green) samples, including the linear regression line (dashed) and correlation coefficient (r = 0.74; R^2 = 0.55). (**B**) Spatial variability of the Cu/Sb ratio across sampling sites for both seasons, illustrating differences in traffic-related source signatures and local emission conditions.

The combined statistical evidence indicates that Mexico City road dust is controlled by at least two principal source domains: (i) geogenic and resuspended mineral particles enriched in V, Cr, Mn, Co, and Ni, derived from regional soils, volcanic materials, and road sediment; and (ii) traffic-related anthropogenic particles enriched in Cu, Sb, Pb, and Cd, primarily associated with brake wear, tire abrasion, and the remobilization of legacy urban contaminants [71,72]. As appears to follow a more heterogeneous behavior, likely influenced by localized or mixed sources. These findings are fully consistent with the spatial hotspot patterns identified in the previous section and highlight the dominant role of vehicular non-exhaust emissions in the metal burden of Mexico City road dust.

3.5. Particle Characterization

Particle size distribution and morphological analyses revealed that Mexico City road dust is composed of a complex assemblage of fine mineral particles, traffic-derived metallic residues, combustion products, engineered materials, and secondary aggregates. The granulometric results (Table 4) showed a clear dominance of fine particles in both sampling seasons, particularly within the 2.5–5 μm SEM-equivalent size classes, which represented the largest proportion of counted particles in most samples. Particles with equivalent diameter between 1 and 2.5 μm commonly accounted for approximately 27–62% of the total particle population, whereas particles between 2.5 and 5 μm contributed an additional ~20–55%, indicating that road dust is strongly enriched in fine particles. When all fractions below 10 μm were combined, they generally represented more than 95% of the counted particles. This result indicates a numerical predominance of fine particles within the analyzed population but should not be interpreted as a mass-size distribution. Coarser particles (10–20 μm) were present in lower proportions, typically below 20%, suggesting that although mechanical fragmentation and local sediment inputs occur, the urban dust matrix is largely dominated by fine material. Quasi-ultrafine particles (<500 nm) were also detected in several samples, particularly during the wet season, reaching up to 1.4% of the counted particles at site S11-wet. Although numerically minor, these particles are environmentally significant because submicron material can remain airborne for prolonged periods [73], penetrate deeply into the alveolar region [74], and exhibit enhanced surface reactivity. Seasonal differences were evident at some locations, with several wet-season samples showing increased 1–2.5 μm abundance compared with their dry-season counterparts (e.g., S6, S35, and S36), possibly reflecting post-rainfall redistribution of fine sediments followed by rapid drying and resuspension. The persistence of fine and quasi-ultrafine particles during both seasons indicates continuous emission, deposition, and re-entrainment processes in Mexico City road dust. This observation is environmentally relevant because deposited fine dust can be readily mobilized by vehicular turbulence, pedestrian activity, and wind action, increasing the probability of inhalation exposure in densely urbanized settings [67,75]. Similar enrichment of fine urban dust fractions has been reported in other traffic-impacted cities of Mexico and elsewhere [6,11].

SEM images demonstrated strong particle heterogeneity in terms of shape, texture, and aggregation state (Figure 8). During the dry season, several distinct particle morphologies were identified sequentially from Figure 8A–F. Spherical Fe-rich particles were frequently observed (Figure 8A), morphologies widely recognized as being consistent with particles generated by high-temperature processes such as brake friction, vehicular abrasion, industrial emissions, and fuel combustion [76,77]. Rod-like Fe-bearing particles were also detected (Figure 8B), compatible with mechanically generated metallic fragments or secondary crystallization products potentially associated with traffic-derived emissions. Angular to sub-rounded Si-rich grains were common (Figure 8C), consistent with crustal dust, pavement abrasion, and construction-derived materials, all typical sources in megac-

ities undergoing intense infrastructure activity [6,78]. Aggregates composed of ultrafine Pb-rich particles were additionally identified (Figure 8D), consistent with anthropogenic contributions potentially linked to historical lead deposition, industrial residues, brake wear, and long-term accumulation in street sediments followed by resuspension [11]. Their occurrence as fine agglomerates is particularly relevant because clustered submicron particles may exhibit enhanced mobility and reactivity in pulmonary environments. Additional Fe-rich spherical particles showed contrasting surface textures between aged and fresh morphologies. Some particles displayed roughened or fractured surfaces (Figure 8E), suggesting oxidation, atmospheric weathering, or secondary coating formation after environmental exposure, whereas others exhibited smooth compact surfaces compatible with recently emitted particles (Figure 8F). The coexistence of fresh and aged Fe-bearing particles indicates continuous emissions combined with particle persistence in the road environment. Wet-season samples also contained morphologically diverse particles (Figure 8G–L). Pb-rich agglomerates remained present (Figure 8G), suggesting that rainfall scavenging does not completely eliminate fine anthropogenic particles and that contaminated sediments can be rapidly reintroduced to road surfaces after drying cycles. Composite Si–O–C particles were identified (Figure 8H), probably representing mixed mineral-anthropogenic particles coated with carbonaceous matter or transformed urban residues. Aged Fe-rich spherical particles were also observed during the wet season (Figure 8I), supporting the persistence of traffic-related metallic emissions throughout the year. In addition, Ca–Fe aluminosilicate particles were detected (Figure 8J), consistent with contributions from mineral dust, cementitious material, or weathered urban debris. Irregular elongated Fe-rich fragments were identified as well (Figure 8K), possibly derived from pavement wear, vehicular components, or construction debris. Finally, clustered smooth carbonaceous aggregates composed of microspherical particles were observed (Figure 8L). These particles are consistent with soot, combustion residues, carbon-rich urban particles, or other C-rich anthropogenic materials [79–81].

Table 4. Grain-size distribution of road dust samples collected in Mexico City during the dry (D) and wet (W) seasons, determined by SEM-EDS. SEM-equivalent projected diameter and number of particles are also reported. Percentages represent particle number distributions derived from SEM counts.

Sample	<500 nm		0.5–1 μm		1–2.5 μm		2.5–5 μm		5–10 μm		10–20 μm		Total	
	Particles	%	Particles	%	Particles	%	Particles	%	Particles	%	Particles	%	Particles	%
S6-D	0	0.0	173	13.2	636	48.8	324	24.9	132	10.1	37	2.8	1302	100
S6-W	0	0.0	0	0.0	683	62.4	299	27.3	85	7.8	27	2.5	1094	100
S11-D	0	0.0	5	0.2	802	29.7	1490	55.2	333	12.3	69	2.6	2699	100
S11-W	20	1.4	35	2.4	393	27.1	706	48.8	230	15.9	64	4.4	1448	100
S14-D	0	0.0	169	10.2	972	58.8	363	21.9	120	7.3	31	1.9	1654	100
S14-W	0	0.0	40	1.8	909	40.2	904	39.9	333	14.7	77	3.4	2263	100
S22-D	0	0.0	22	1.4	881	56.7	444	28.6	172	11.1	34	2.2	1553	100
S22-W	4	0.2	125	7.3	933	54.2	492	28.6	142	8.2	25	1.4	1721	100
S29-D	0	0.0	61	4.8	621	49.2	411	32.6	155	12.3	13	1.0	1261	100
S29-W	0	0.0	5	0.3	556	37.8	583	39.7	256	17.4	70	4.8	1470	100
S33-D	0	0.0	50	4.6	459	42.6	363	33.7	163	15.1	43	4	1078	100
S33-W	5	0.4	139	12.3	554	48.8	323	28.5	104	9.2	9	0.8	1134	100
S35-D	1	0.1	41	3.6	484	42.5	417	36.6	180	15.8	15	1.3	1138	100
S35-W	0	0.0	28	1.3	1218	56.5	688	31.9	193	8.9	29	1.3	2156	100
S36-D	0	0.0	38	3	579	45.5	458	36	165	13	33	2.6	1273	100
S36-W	0	0.0	155	11.6	812	60.9	271	20.3	84	6.3	12	0.9	1334	100

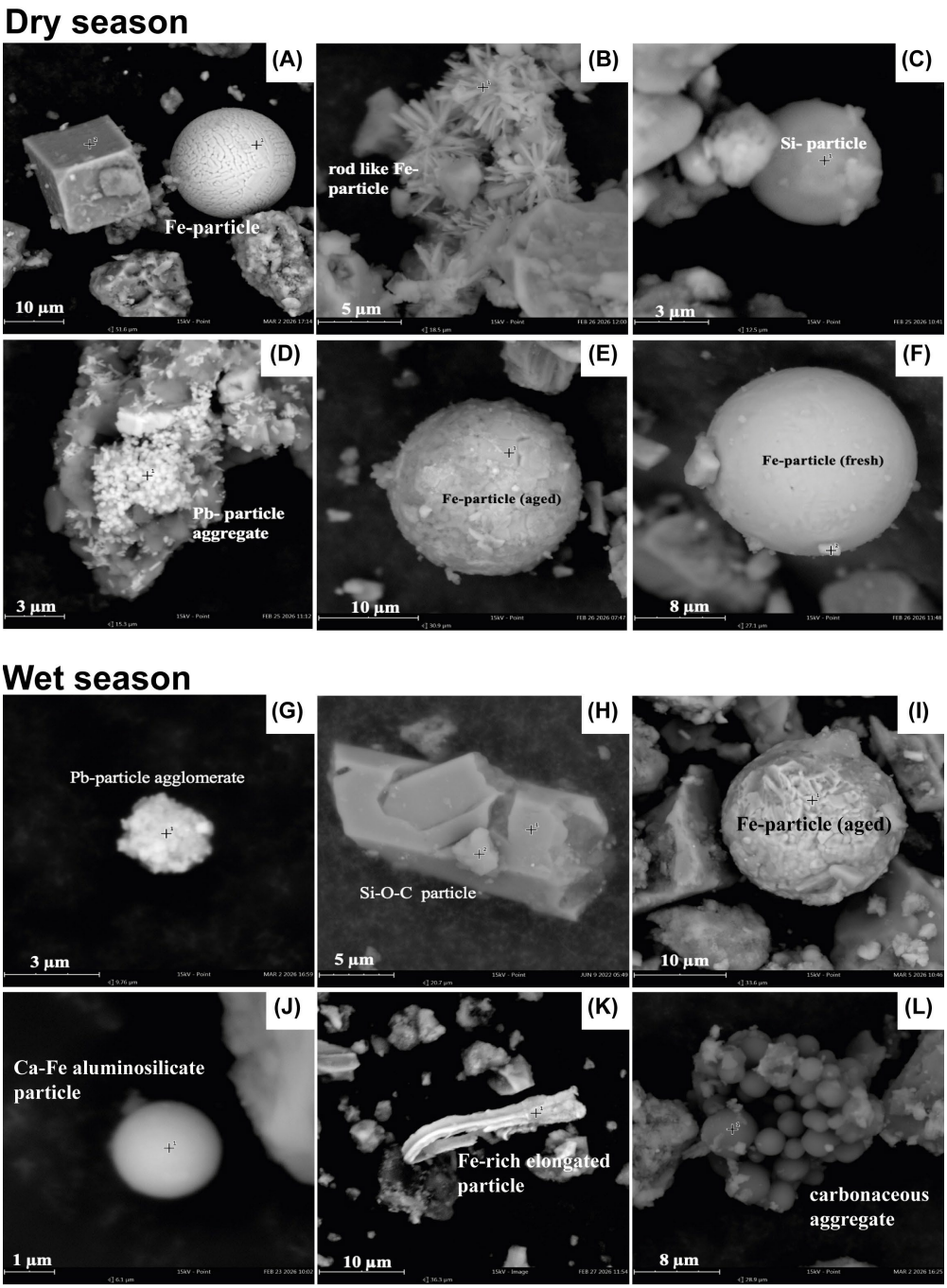


Figure 8. Representative SEM images of road dust particles collected in Mexico City during the dry and wet seasons, illustrating the diversity of particle morphology, texture, and probable sources. (**A**) Spherical Fe-rich particle and cubic particle; (**B**) rod-like Fe-rich particle; (**C**) spherical Si-rich particle; (**D**) Pb-rich particle aggregate; (**E**) aged Fe-rich particle; (**F**) fresh Fe-rich particle; (**G**) Pb-rich particle agglomerate; (**H**) Si–O–C particle; (**I**) aged Fe-rich particle; (**J**) Ca–Fe aluminosilicate particle; (**K**) Fe-rich elongated particle; (**L**) carbonaceous aggregate.

Representative EDS spectra (Figure S4) confirmed the compositional diversity inferred from morphology. Fe was one of the most recurrent elements, supporting the importance of brake wear, steel abrasion, and combustion-related particles. Si, Al, Ca, Mg, and O were abundant in angular grains, indicating aluminosilicates, cementitious material, soil minerals, and construction dust. Pb-bearing particles were confirmed in localized aggregates, while mixed assemblages containing Fe, Cu, and other PTEs suggest complex multi-source urban emissions. C-rich particles were also identified, compatible with soot, carbonaceous

urban particles, or carbon-rich surface coatings formed during atmospheric aging [5]. The coexistence of metallic spherules, Pb-rich aggregates, silicate grains, and carbonaceous particles demonstrates that Mexico City road dust is not merely geogenic sediment but rather a chemically and physically transformed urban particulate reservoir integrating emissions from traffic, infrastructure wear, construction activity, atmospheric deposition, and urban waste fragmentation. This interpretation agrees with the strong geochemical enrichment observed for Cu, Sb, Pb, and Cd, as well as with the source associations derived from PCA and correlation analyses. In particular, the recurrent presence of Fe-rich spherules and Pb-bearing fine particles is consistent with an important contribution from non-exhaust vehicular emissions, especially brake and mechanical wear processes, although other urban and industrial sources may also contribute to these particle types [67,77].

From a health perspective, particle toxicity depends not only on total elemental concentration but also on size, morphology, and surface reactivity. Fine and ultrafine particles can penetrate deeply into the respiratory tract, while irregular surfaces and aggregated nanometric material may favor dissolution kinetics or oxidative interactions in lung fluids [11,75]. Therefore, the particle evidence presented here provides an important mechanistic link between metal enrichment in road dust and the inhalation-related risks.

3.6. Health Risk Assessment and Lung Bioaccessibility

3.6.1. Non-Carcinogenic and Carcinogenic Risk

The health risk assessment (Table 5) showed clear differences between adults and children, with children representing the most sensitive receptor group because of their lower body weight and higher dust ingestion rates relative to body mass [82]. For adults, the cumulative non-carcinogenic hazard index (HI) remained below the threshold value of 1 in both seasons, with values of 0.42 for the dry season and 0.49 for the wet season. These values suggest that, under the exposure assumptions used in this study, non-carcinogenic risk for adults is low. In contrast, the cumulative HI values for children exceeded the safety threshold in both seasons, reaching 3.85 during the dry season and 4.60 during the wet season. These results indicate a potential concern under the conservative exposure assumptions adopted in this study and suggest that children represent the most sensitive receptor group within the evaluated scenario. Among the individual PTEs, Pb was the main contributor to the calculated non-carcinogenic risk, especially for children, with HI values of 1.2 in the dry season and 1.5 in the wet season. These values exceeded the conventional threshold of 1. However, Pb-related HI values should be interpreted with caution because lead toxicology is commonly evaluated using blood-lead modelling approaches rather than threshold-based reference doses [83]. Therefore, the Pb-related risk estimates presented here should be considered screening-level indicators of potential exposure rather than definitive measures of health risk. Other elements contributed to the cumulative risk but did not individually exceed the threshold. In children, Cr showed HI values of 0.78 and 0.82 for the dry and wet seasons, respectively, followed by Co (0.56–0.68), Mn (0.48–0.49), As (0.25–0.57), Sb (0.21–0.24), and V (0.18–0.21). The higher cumulative HI observed during the wet season was mainly associated with increases in Pb, As, Co, and V. Although adults showed the same general element ranking, all individual HI values were lower than 1, confirming that children are the most exposed population group under the evaluated scenario.

The CR assessment (Table 5) also showed higher values for children than for adults. For adults, TCR values were 6.3×10^{-5} in the dry season and 6.9×10^{-5} in the wet season. These values fall within the commonly accepted or tolerable risk range of 1×10^{-6} to 1×10^{-4}. In contrast, children showed TCR values of 1.2×10^{-4} and 1.3×10^{-4} for the dry and wet seasons, respectively, slightly exceeding the upper acceptable limit of 1×10^{-4}. This result suggests that long-term exposure to road dust may represent a carcinogenic

concern for children, particularly in areas with elevated concentrations of carcinogenic PTEs. The carcinogenic risk was largely dominated by Cr, followed by As, whereas Ni, Cd, and Pb showed comparatively minor contributions. This pattern should be interpreted with caution because the risk calculation uses total Cr concentrations and does not distinguish between Cr(III) and Cr(VI), the latter being the more toxic and carcinogenic species. Consequently, the chromium-related carcinogenic risk estimates should be regarded as conservative maximum-risk scenarios. Nevertheless, the high contribution of Cr highlights the need to consider both concentration and chemical speciation in future risk assessments.

Table 5. Non-carcinogenic hazard index (HI) and total carcinogenic risks (TCR) for adults and children based on exposure to PTEs in road dust during dry and wet season in Mexico City, Mexico.

	V	Cr	Mn	Co	Ni	Cu	As	Cd	Sb	Pb
Non-carcinogenic										
Dry season										
Adults	1.9×10^{-2}	8.5×10^{-2}	5.6×10^{-2}	6.0×10^{-2}	3.6×10^{-3}	5.5×10^{-3}	2.7×10^{-2}	1.5×10^{-3}	2.6×10^{-2}	1.3×10^{-1}
Children	1.8×10^{-1}	7.8×10^{-1}	4.9×10^{-1}	5.6×10^{-1}	3.3×10^{-2}	5.1×10^{-2}	2.5×10^{-1}	1.3×10^{-2}	2.4×10^{-1}	1.2×10^{0}
Wet Season										
Adults	2.2×10^{-2}	8.9×10^{-2}	5.6×10^{-2}	7.3×10^{-2}	3.7×10^{-3}	4.7×10^{-3}	6.1×10^{-2}	1.5×10^{-3}	2.2×10^{-2}	1.6×10^{-1}
Children	2.1×10^{-1}	8.2×10^{-1}	4.8×10^{-1}	6.8×10^{-1}	3.5×10^{-2}	4.4×10^{-2}	5.7×10^{-1}	1.2×10^{-1}	2.1×10^{-1}	1.5×10^{0}
Carcinogenic										
Dry season										
Adults		5.5×10^{-5}	-	-	3.8×10^{-9}	-	7.3×10^{-6}	5.1×10^{-10}	-	6.7×10^{-7}
Children	-	1.0×10^{-4}	-	-	1.3×10^{-9}	-	1.4×10^{-5}	1.8×10^{-10}	-	1.3×10^{-6}
Wet Season										
Adults	-	5.7×10^{-5}	-	-	3.4×10^{-9}	-	1.2×10^{-5}	5.0×10^{-10}	-	8.3×10^{-7}
Children	-	1.1×10^{-4}	-	-	1.4×10^{-9}	-	2.2×10^{-5}	1.8×10^{-10}	-	1.5×10^{-6}

3.6.2. Lung Bioaccessibility

The lung bioaccessibility results (Figure 9 and Table S7) provided additional insight into the fraction of PTEs that may become soluble under acidic intracellular lung conditions simulated by ALF. Bioaccessibility varied markedly among elements and between individual samples, indicating that PTE mobility is controlled not only by total concentration but also by particle mineralogy, surface reactivity, grain size, and association with specific anthropogenic or geogenic phases. Elements such as V and Mn showed consistently low bioaccessibility in both seasons. V showed median values close to 1%, while Mn was generally between 2 and 5%, suggesting that these elements were mostly hosted in relatively insoluble mineral phases. Pb also showed limited bioaccessibility, with median values of 7.4% in the dry season and 5.9% in the wet season. This is important because Pb showed high total concentrations and was the main driver of non-carcinogenic risk, but only a small fraction was mobilized in ALF. This apparent contrast reflects the different basis of the two assessments. The health-risk calculations were performed using total Pb concentrations and toxicity-weighted exposure models, whereas the bioaccessibility results represent only the fraction potentially dissolved under simulated lysosomal conditions. Consequently, Pb may dominate the risk assessment because of its elevated concentrations and toxicological weighting, even though its ALF solubility is relatively low. Therefore, total Pb concentration represents a conservative exposure metric, whereas ALF bioaccessibility suggests that only part of the total Pb pool may become soluble under lysosomal conditions. In contrast, Ni and Cu showed the highest and most variable bioaccessibility values. Ni presented median bioaccessibility values of 30.7% in the dry season and 23.8% in the wet season, with some samples reaching 100%. Cu showed median values close to 11% in both seasons but also reached 100% in some samples. These high values indicate that, in specific sites, Ni and Cu may occur in relatively labile phases that are easily dissolved in acidic lung fluid. This behavior is consistent with the occurrence of traffic-related and mechanically derived particles, including brake wear residues, metallic particles, and mixed

Fe–Cu-bearing assemblages observed by SEM-EDS. The large variability observed for Ni and Cu suggests that their bioaccessibility is strongly source-dependent and may reflect localized inputs rather than a uniform citywide pattern. Cr and Co showed intermediate behavior. Cr had low median values but a broad range, reaching up to 29.9% in the dry season and 28.0% in the wet season. Co showed median values of 6.9% in the dry season and 4.0% in the wet season, with maximum values of 11.4% and 12.9%, respectively. These results suggest that most Cr and Co are present in relatively resistant phases, although a subset of particles contains more soluble forms. As was detected in only a limited number of ALF extracts, with bioaccessibility values between 9.3 and 12.9% in the dry season and 1.1 and 15.5% in the wet season. Therefore, the interpretation of As bioaccessibility should be considered preliminary because of the low number of quantifiable values. Cd and Sb were not consistently quantified in ALF extracts, preventing reliable calculation of their bioaccessible percentages. Seasonal differences in bioaccessibility were generally less systematic than differences in total concentrations. Most elements showed comparable median values between dry and wet seasons, although some site-specific variations were evident. This suggests that the solubility of PTEs in ALF is mainly controlled by particle composition and source-related mineral phases rather than by season alone [17]. However, seasonal processes may still influence bioaccessibility indirectly by modifying the road dust pool through wash-off, particle aging, oxidation, deposition of fresh emissions, and redistribution of fine material after rainfall [11]. For example, the presence of highly bioaccessible Ni and Cu in both seasons indicates continuous input of labile traffic-related particles, while the persistence of Pb-rich aggregates and Fe-bearing particles observed by SEM-EDS supports the interpretation of year-round non-exhaust vehicular emissions.

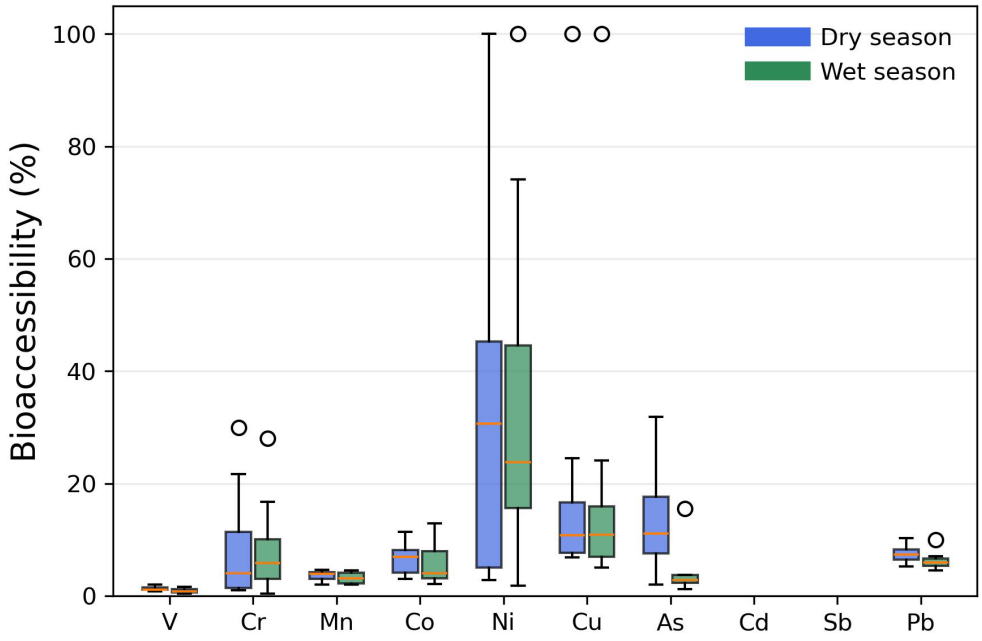


Figure 9. Lung bioaccessibility (%) of PTEs in Mexico City road dust extracted with artificial lysosomal fluid (ALF) during the dry and wet seasons. Orange lines indicate the median values, and circles represent outliers.

An additional inhalation-risk scenario was calculated using ALF-bioaccessible concentrations to evaluate the influence of pulmonary metal mobility on exposure estimates (Table S8). Bioaccessibility-adjusted inhalation HQ values were substantially lower than those obtained using total concentrations for both adults and children. Bioaccessibility-adjusted inhalation HQ values ranged from 5.26×10^{-9} to 1.46×10^{-6} for adults and from 6.44×10^{-9} to 2.04×10^{-6} for children. Cr remained the largest contributor to in-

halation risk, with HQ values of 1.46×10^{-6} and 1.42×10^{-6} for adults and 2.04×10^{-6} and 1.98×10^{-6} for children during the dry and wet seasons, respectively. However, all bioaccessibility-adjusted HQ values remained several orders of magnitude below the threshold value of 1. These results indicate that only a limited fraction of the total metal burden is potentially available under simulated pulmonary conditions and suggest that inhalation risks estimated from total concentrations may overestimate actual pulmonary exposure. The conventional USEPA risk assessment framework is based on total contaminant concentrations and therefore provides conservative screening-level estimates of potential exposure, whereas the ALF-based calculations offer a complementary and more realistic estimate of the fraction potentially available for interaction with lung tissues after particle deposition.

Taken together, the health risk and bioaccessibility results show that total PTE concentrations and bioaccessible fractions provide complementary information. The health risk assessment based on total concentrations identified Pb, Cr, As, Co, and Mn as the main contributors to cumulative non-carcinogenic risk, with children exceeding the acceptable HI threshold in both seasons. The carcinogenic risk assessment further indicated that children slightly exceeded the upper acceptable risk limit, mainly because of Cr and As. In contrast, ALF bioaccessibility showed that the most soluble elements were not necessarily those with the highest total concentrations or highest risk contribution. For instance, Pb was the dominant non-carcinogenic risk driver but showed relatively low lung bioaccessibility, whereas Ni and Cu showed higher mobility in ALF despite lower health-risk contributions. This contrast emphasizes the importance of integrating total concentration, risk modeling, SEM-EDS particle characterization, and in vitro bioaccessibility to better understand the potential health implications of road dust exposure in Mexico City. These findings are consistent with previous studies showing that inhalation bioaccessibility can vary widely among urban particles and that risk evaluations based only on total concentrations may overestimate or underestimate the biologically relevant fraction depending on the element and its host phase [21,22,84,85].

3.7. Limitations of the Study

Although this study provides an integrated assessment of seasonal geochemistry, contamination levels, particle characteristics, health risk, and lung bioaccessibility of Mexico City road dust, some limitations should be acknowledged. First, source identification was based on the combined interpretation of spatial patterns, enrichment factors, correlation analysis, PCA, and SEM–EDS observations. While this multi-proxy approach provides robust evidence for dominant traffic-related and urban anthropogenic inputs, it does not allow definitive discrimination among specific Pb sources. In particular, Pb may originate from multiple overlapping contributors, including brake wear, industrial emissions, resuspension of historically contaminated sediments, demolition materials, and legacy deposits derived from the historical use of leaded gasoline. Future studies incorporating Pb isotopic ratios (e.g., $^{206}Pb/^{207}Pb$, $^{208}Pb/^{206}Pb$) would substantially improve source identification by distinguishing between contemporary and historical emission signatures. A second limitation relates to mineralogical characterization of the dust matrix. SEM–EDS provided valuable information on particle morphology and elemental composition, but it does not fully resolve crystalline versus amorphous phases nor the specific mineral hosts controlling metal retention and dissolution behavior. Because lung bioaccessibility is strongly influenced by mineralogy, oxidation state, and metal association with reactive surface phases, complementary analyses such as X-ray diffraction (XRD), Raman spectroscopy, or synchrotron-based techniques would help identify the phases governing PTE mobility under simulated pulmonary conditions. This would be particularly relevant for elements such

as Pb, Cr, Fe, and Mn, whose solubility may vary substantially depending on whether they occur as oxides, silicates, carbonates, adsorbed coatings, or mixed anthropogenic particles.

Despite these limitations, the combination of chemical analysis, geochemical indices, spatial mapping, multivariate statistics, SEM–EDS particle characterization, health risk modeling, and ALF bioaccessibility testing provides a robust framework for understanding road dust contamination and potential human exposure in one of the world's largest megacities.

4. Conclusions

This study provides an integrated assessment of the seasonal variability, contamination levels, source identification, particle characteristics, lung bioaccessibility, and health risk of PTEs in Mexico City road dust.

The results indicate that road dust in this megacity is strongly influenced by anthropogenic emissions, particularly traffic-related non-exhaust sources, although geogenic contributions remain important for some elements. Seasonal differences were observed, but they were generally secondary to the persistent urban contamination signal. Geochemical indices, spatial patterns, correlation analysis, PCA, and SEM–EDS observations consistently identified two contrasting groups: a predominantly geogenic association (V, Cr, Mn, Co, and Ni) and a traffic-related association enriched in Cu, Sb, Pb, and Cd. Among the analyzed elements, Sb showed the highest contamination levels, while Cd represented the greatest ecological concern. Recurrent hotspots were concentrated in the northern, northeastern, and central sectors of the city, reflecting the influence of intense urban activity and traffic emissions. Health-risk assessment indicated acceptable risks for adults, whereas children exhibited the highest screening-level risk estimates under the conservative exposure assumptions adopted in this study. Lung bioaccessibility results further demonstrated that total concentration alone does not necessarily reflect potential mobility or toxicity, highlighting the importance of integrating chemical, mineralogical, and bioaccessibility information when evaluating urban exposure.

Road dust represents a persistent reservoir of traffic-related contaminants in Mexico City and highlights the importance of mitigation strategies focused on non-exhaust vehicular emissions and road dust management.

Supplementary Materials: The following supporting information can be downloaded at: https://www.mdpi.com/article/10.3390/environments13070372/s1. Table S1: The quality control of the ICP-MS measurements was verified using the certified reference material SRM-1648a; Table S2: Chemical composition of ALF solutions used for in vitro lung bioaccessibility test [6]; Table S3: Parameters and values for human health risk calculation [43,44]; Table S4: Reference dose (RfD, mg kg^{-1} day^{-1}) values for non-carcinogenic risk and slope factor (SF, kg mg^{-1} day^{-1}) values for carcinogenic risk [31,32,44,45]; Table S5: Wilcoxon signed-rank test comparing PTE concentrations in road dust between the dry and wet seasons at the same sampling locations (n = 37). Significant seasonal differences are indicated by $p < 0.05$; Table S6: Potentially Toxic Element (PTE) concentrations (mg kg^{-1}) in the <20 μm fraction of road dust collected during the dry and wet sampling seasons in Mexico City; Table S7: Lung bioaccessibility (%) of PTEs from Mexico City road dust during dry and wet season; Table S8: Bioaccessibility-adjusted inhalation hazard quotients (HQinh-adj) calculated using ALF-extractable concentrations of PTEs in road dust from Mexico City for adults and children during the dry and wet seasons; Figure S1: Percentage of sampling sites in Mexico City road dust exceeding the local background concentration for each PTE during the dry season (blue bars) and wet season (orange bars). Values above the bars indicate the proportion (%) of sites with concentrations higher than the background reference, emphasizing the widespread enrichment of Cu, Sb, Pb, and Cd in both seasons; Figure S2: Boxplots of PTE concentrations in Mexico City road dust for the dry season (blue), wet season (green), and local background reference (red horizontal lines). The left panel

shows Mn separately because of its higher concentration range, whereas the right panel presents V, Cr, Co, Ni, Cu, As, Cd, Sb, and Pb. Boxes represent the interquartile range, center lines indicate medians, and whiskers show data dispersion excluding outliers; Figure S3: Seasonal PCA biplots showing the distribution of PTEs in Mexico City road dust during the dry season and wet season; Figure S4: Representative semi-quantitative EDS spectra of selected road dust particles collected during the dry and wet seasons in Mexico City. Spectra correspond to particles shown in Figure 8 and illustrate the compositional variability of Fe-rich, Pb-bearing, silicate, and carbonaceous particles.

Author Contributions: Conceptualization, B.S. and D.M.M.-F.; methodology, B.S., D.M.M.-F. and C.I.; software, B.S.; validation, B.S., D.M.M.-F., C.I., O.M.-B., D.V.-F., B.G.-G., F.B.-R. and E.H.-Á.; formal analysis, B.S., D.M.M.-F., C.I., O.M.-B., B.G.-G., F.B.-R. and E.H.-Á.; investigation, B.S., D.M.M.-F., C.I., O.M.-B., D.V.-F., B.G.-G. and F.B.-R.; resources, D.M.M.-F., C.I. and O.M.-B.; data curation, B.S. and D.M.M.-F.; writing—original draft preparation, B.S.; writing—review and editing, B.S., D.M.M.-F., C.I., O.M.-B., D.V.-F., B.G.-G., F.B.-R. and E.H.-Á.; visualization, B.S. and B.G.-G.; supervision, D.M.M.-F. and O.M.-B.; project administration, D.M.M.-F. All authors have read and agreed to the published version of the manuscript.

Funding: This research was funded by the National Council for Humanities, Science and Technology in Mexico (CONAHCyT) Grant A1-S-29697 and PRONACES 317557 to Diana Meza-Figueroa.

Data Availability Statement: Data is contained within the article or Supplementary Material.

Acknowledgments: The authors gratefully acknowledge María Margarita Martínez Rodríguez for her assistance during the ICP-MS analyses of the bioaccessible fraction carried out at the Sistema de Laboratorios Especializados de Ciencias de la Tierra (SLE-CT), Centro de Investigación Científica y de Educación Superior de Ensenada (CICESE), Baja California, Mexico. The authors also acknowledge the Laboratorio de ICP-MS at the Instituto de Geofísica, UNAM, for analytical support.

Conflicts of Interest: The authors declare no conflicts of interest.

References

1. Mostafa, M.T.; El-Nady, H.; Gomaa, R.M.; Abdelgawad, H.F.; Abdelhafiz, M.A.; Abd Elraouf Salman, S.; Khalifa, I.H. Urban geochemistry of heavy metals in road dust from Cairo megacity, Egypt: Enrichment, sources, contamination, and health risks. *Environ. Earth Sci.* **2024**, *83*, 37. [CrossRef]
2. Naraki, H.; Keshavarzi, B.; Zarei, M.; Moore, F.; Abbasi, S.; Kelly, F.J.; Oliete Dominguez, A.; Jaafarzadeh, N. Urban street dust in the Middle East oldest oil refinery zone: Oxidative potential, source apportionment, and health risk assessment of potentially toxic elements. *Chemosphere* **2021**, *268*, 128825. [CrossRef] [PubMed]
3. Tashakor, M.; Modabberi, S.; Argyraki, A. Assessing the contamination level, sources and risk of potentially toxic elements in urban soil and dust of Iranian cities using secondary data of published literature. *Environ. Geochem. Health* **2022**, *44*, 645–675. [CrossRef] [PubMed]
4. Das, M.; Proshad, R.; Chandra, K.; Islam, M.; Abdullah Al, M.; Baroi, A.; Idris, A.M. Heavy metals contamination, receptor model-based sources identification, sources-specific ecological and health risks in road dust of a highly developed city. *Environ. Geochem. Health* **2023**, *45*, 8633–8662. [CrossRef] [PubMed]
5. Berrellez-Reyes, F.; Schiavo, B.; Gonzalez-Grijalva, B.; Angulo-Molina, A.; Meza-Figueroa, D. Characterization of soot and crystalline atmospheric ultrafine particles. *Environ. Pollut.* **2025**, *364*, 125314. [CrossRef] [PubMed]
6. Meza-Figueroa, D.; Barboza-Flores, M.; Romero, F.M.; Acosta-Elias, M.; Hernández-Mendiola, E.; Maldonado-Escalante, F.; Pérez-Segura, E.; González-Grijalva, B.; Meza-Montenegro, M.; García-Rico, L.; et al. Metal bioaccessibility, particle size distribution and polydispersity of playground dust in synthetic lysosomal fluids. *Sci. Total Environ.* **2020**, *713*, 136481. [CrossRef] [PubMed]
7. Chen, L.; Yousaf, M.; Xu, J.; Ma, X.; Zhou, X.; Li, G.; Symonds, J.; Chen, R.; Tang, S.; Salehi, F.; et al. Ultrafine particles deposition in human respiratory tract: Experimental measurement and modeling. *Ecotoxicol. Environ. Saf.* **2025**, *295*, 118123. [CrossRef] [PubMed]
8. Liu, Y.; Xu, F.; Liu, W.; Liu, X.; Wang, D. Characteristics, sources, exposure, and health effects of heavy metals in atmospheric particulate matter. *Curr. Pollut. Rep.* **2025**, *11*, 16. [CrossRef]
9. Guney, M.; Chapuis, R.P.; Zagury, G.J. Lung bioaccessibility of contaminants in particulate matter of geological origin. *Environ. Sci. Pollut. Res.* **2016**, *23*, 24422–24434. [CrossRef] [PubMed]

10. Ivaneev, A.I.; Brzhezinskiy, A.S.; Karandashev, V.K.; Ermolin, M.S.; Fedotov, P.S. Assessment of sources, environmental, ecological, and health risks of potentially toxic elements in urban dust of Moscow megacity, Russia. *Chemosphere* **2023**, *321*, 138142. [CrossRef] [PubMed]
11. Schiavo, B.; Meza-Figueroa, D.; Vizuete-Jaramillo, E.; Robles-Morua, A.; Angulo-Molina, A.; Reyes-Castro, P.A.; Inguaggiato, C.; Gonzalez-Grijalva, B.; Pedroza-Montero, M. Oxidative potential of metal-polluted urban dust as a potential environmental stressor for chronic diseases. *Environ. Geochem. Health* **2023**, *45*, 3229–3250. [CrossRef] [PubMed]
12. Čakmak, D.; Perović, V.; Kresović, M.; Pavlović, D.; Pavlović, M.; Mitrović, M.; Pavlović, P. Sources and a health risk assessment of potentially toxic elements in dust at children's playgrounds with artificial surfaces: A case study in Belgrade. *Arch. Environ. Contam. Toxicol.* **2020**, *78*, 190–205. [CrossRef] [PubMed]
13. Li, S.; Bi, X.; Li, Z.; Wang, H.; Li, X.; Feng, X.; Sun, G.; Chen, J.; Meng, B. Heavy metal(loid)s contamination in ground dust and associated health risks at a former indigenous zinc smelting area. *Int. J. Environ. Res. Public Health* **2021**, *18*, 893. [CrossRef] [PubMed]
14. Men, C.; Liu, R.; Wang, Q.; Guo, L.; Shen, Z. The impact of seasonal varied human activity on characteristics and sources of heavy metals in metropolitan road dusts. *Sci. Total Environ.* **2018**, *637–638*, 844–854. [CrossRef] [PubMed]
15. Duan, T.; Liu, S.; Wang, D.; Feng, J.; Song, N.; Yu, Y.; Li, Y. Seasonal variation and sources of heavy metals in urban street dusts and river sediments of Dongluo River watershed in Ji'nan City, China. *KSCE J. Civ. Eng.* **2020**, *24*, 1400–1410. [CrossRef]
16. Zhang, L.; Qian, J.; Liu, J.; Niu, K.; Zhang, H. Seasonal dynamics and source apportionment of heavy metals in road dust: A case study of Liuzhou, China. *Sustainability* **2024**, *16*, 10051. [CrossRef]
17. Schiavo, B.; Meza-Figueroa, D.; Pedroza-Montero, M.; Vidal-Solano, J.; González-Grijalva, B.; Navarro-Espinoza, S.; Romero, F.; Hernández, E.; Gutiérrez-Ruiz, M.E.; Ceniceros-Gómez, A.E. In vitro assessment oral and respiratory bioaccessibility of Mn in school dust: Insight of seasonality in a semiarid environment. *Appl. Geochem.* **2021**, *134*, 105102. [CrossRef]
18. Ivaneev, A.I.; Brzhezinskiy, A.S.; Karandashev, V.K.; Ermolin, M.S.; Fedotov, P.S. Seasonal variability of the elemental composition and ecological risks of urban dust of Moscow megacity. *Geochem. Int.* **2026**, *64*, 220–235. [CrossRef]
19. Wiseman, C.L.S.; Levesque, C.; Rasmussen, P.E. Characterizing the sources, concentrations and resuspension potential of metals and metalloids in the thoracic fraction of urban road dust. *Sci. Total Environ.* **2021**, *786*, 147467. [CrossRef] [PubMed]
20. Jia, B.; Tian, Y.; Dai, Y.; Chen, R.; Zhao, P.; Chu, J.; Feng, X.; Feng, Y. Seasonal variation of dissolved bioaccessibility for potentially toxic elements in size-resolved PM: Impacts of bioaccessibility on inhalable risk and uncertainty. *Environ. Pollut.* **2022**, *307*, 119551. [CrossRef] [PubMed]
21. Boim, A.G.; Patinha, C.; Wragg, J.; Cave, M.; Alleoni, L.R.F. Respiratory bioaccessibility and solid phase partitioning of potentially harmful elements in urban environmental matrices. *Sci. Total Environ.* **2021**, *765*, 142791. [CrossRef] [PubMed]
22. Expósito, A.; Markiv, B.; Ruiz-Azcona, L.; Santibáñez, M.; Fernández-Olmo, I. Understanding how methodological aspects affect the release of trace metal(loid)s from urban dust in inhalation bioaccessibility tests. *Chemosphere* **2021**, *267*, 129181. [CrossRef] [PubMed]
23. Alam, M.J.; Rappenglueck, B.; Retama, A.; Rivera-Hernández, O. Investigating the complexities of VOC sources in Mexico City in the years 2016–2022. *Atmosphere* **2024**, *15*, 179. [CrossRef]
24. Instituto Nacional de Estadística y Geografía (INEGI). Censo de Población y Vivienda 2020: Resultados de la Ciudad de México. INEGI 2021. Available online: https://www.inegi.org.mx/contenidos/saladeprensa/boletines/2021/EstSociodemo/ResultCenso2020_CdMx.pdf (accessed on 17 February 2026).
25. Estrada, F.; Martínez-Arroyo, A.; Fernández-Eguiarte, A.; Luyando, E.; Gay, C. Defining climate zones in Mexico City using multivariate analysis. *Atmósfera* **2009**, *22*, 175–193.
26. Behzadi, F.; Wasti, A.; Rahat, S.H.; Tracy, J.N.; Ray, P.A. Analysis of the climate change signal in Mexico City given disagreeing data sources and scattered projections. *J. Hydrol. Reg. Stud.* **2020**, *27*, 100662. [CrossRef]
27. López-Espinoza, E.D.; Fuentes-Mariles, O.A.; Herrera-Moro, D.R.; Gómez-Ramos, O.; Novelo-Casanova, D.A.; Zavala-Hidalgo, J. Daily precipitation data for the Mexico City Metropolitan Area from 1930 to 2015. *Data* **2022**, *7*, 88. [CrossRef]
28. Arce, J.L.; Layer, P.W.; Macías, J.L.; Morales-Casique, E.; García-Palomo, A.; Jiménez-Domínguez, F.J. Geology and stratigraphy of the Mexico Basin (Mexico City), central Trans-Mexican Volcanic Belt. *J. Maps* **2019**, *15*, 320–332. [CrossRef]
29. Juárez-Camarena, M.; Auvinet-Guichard, G.; Méndez-Sánchez, E. Geotechnical zoning of Mexico Valley subsoil. *Ing. Investig. Tecnol.* **2016**, *17*, 297–308. [CrossRef]
30. Jáuregui, E. Impact of land-use changes on the climate of the Mexico City region. *Investig. Geogr.* **2004**, *55*, 46–60. Available online: https://www.scielo.org.mx/pdf/igeo/n55/n55a4.pdf (accessed on 14 March 2026).
31. Schiavo, B.; Meza-Figueroa, D.; Morton-Bermea, O.; Angulo-Molina, A.; González-Grijalva, B.; Armienta-Hernández, M.A.; Inguaggiato, C.; Berrellez-Reyes, F.; Valera-Fernández, D. Metal(loid) bioaccessibility and risk assessment of ashfall deposit from Popocatépetl volcano, Mexico. *Environ. Geochem. Health* **2024**, *46*, 354. [CrossRef] [PubMed]

32. Schiavo, B.; Valenzuela-Meza, J.; Valera-Fernández, D.; Inguaggiato, C.; Meza-Figueroa, D.; Morton-Bermea, O. Spatial distribution, contamination levels, and health risk of potentially toxic elements in surface soils of an industrial–urban area in northwestern Mexico: A case study from La Paz, Baja California Sur. *Environ. Geochem. Health* **2026**, *48*, 36. [CrossRef] [PubMed]
33. Alghamdi, A.G.; El-Saeid, M.H.; Alzahrani, A.J.; Ibrahim, H.M. Heavy metal pollution and associated health risk assessment of urban dust in Riyadh, Saudi Arabia. *PLoS ONE* **2022**, *17*, e0261957. [CrossRef] [PubMed]
34. Dange, S.; Arumugam, K.; Vijayaraghavalu, S.S. Geochemical insights into heavy metal contamination and health hazards in Palar River Basin: A pathway to sustainable solutions. *Ecol. Indic.* **2024**, *166*, 112568. [CrossRef]
35. Hakanson, L. An ecological risk index for aquatic pollution control. *Water Res.* **1980**, *14*, 975–1001. [CrossRef]
36. Müller, G. Index of geoaccumulation in sediments of the Rhine River. *GeoJournal* **1969**, *2*, 108–118. Available online: https://www.scirp.org/reference/ReferencesPapers?ReferenceID=1803049 (accessed on 22 February 2026).
37. Lv, Y.; Kabanda, G.; Chen, Y.; Wu, C.; Li, W. Spatial distribution and ecological risk assessment of heavy metals in manganese (Mn) contaminated site. *Front. Environ. Sci.* **2022**, *10*, 942544. [CrossRef]
38. Zhang, C. Using multivariate analyses and GIS to identify pollutants and their spatial patterns in urban soils in Galway, Ireland. *Environ. Pollut.* **2006**, *142*, 501–511. [CrossRef] [PubMed]
39. Hussain, A.; Bangroo, S.A.; Muslim, M. Assessment of soil contamination using remote sensing and spatial techniques. In *Geospatial Analytics for Environmental Pollution Modeling*; Mushtaq, F., Farooq, M., Mukherjee, A.B., Ghosh Nee Lala, M., Eds.; Springer: Cham, Switzerland, 2023; pp. 249–266. [CrossRef]
40. Meza-Figueroa, D.; Berrellez-Reyes, F.; Schiavo, B.; Morton-Bermea, O.; Gonzalez-Grijalva, B.; Inguaggiato, C.; Silva-Campa, E. Tracking fine particles in urban and rural environments using honey bees as biosamplers in Mexico. *Chemosphere* **2024**, *363*, 142881. [CrossRef] [PubMed]
41. Colombo, C.; Monhemius, A.J.; Plant, J.A. Platinum, palladium and rhodium release from vehicle exhaust catalysts and road dust exposed to simulated lung fluids. *Ecotoxicol. Environ. Saf.* **2008**, *71*, 722–730. [CrossRef] [PubMed]
42. Boisa, N.; Elom, N.; Dean, J.R.; Deary, M.E.; Bird, G.; Entwistle, J.A. Development and application of an inhalation bioaccessibility method (IBM) for lead in the PM10 size fraction of soil. *Environ. Int.* **2014**, *70*, 132–142. [CrossRef] [PubMed]
43. USEPA. *Risk Assessment Guidance for Superfund: Volume III—Part A, Process for Conducting Probabilistic Risk Assessment*; U.S. Environmental Protection Agency: Washington, DC, USA, 2001. Available online: https://www.epa.gov/sites/default/files/2015-09/documents/rags3adt_complete.pdf (accessed on 14 March 2026).
44. USEPA. *Supplemental Guidance for Developing Soil Screening Levels for Superfund Sites*; U.S. Environmental Protection Agency, Office of Emergency and Remedial Response: Washington, DC, USA, 2002. Available online: https://nepis.epa.gov/Exe/ZyPDF.cgi/91003IJK.PDF?Dockey=91003IJK.PDF (accessed on 14 March 2026).
45. USEPA. *Integrated Risk Information System (IRIS)*; U.S. Environmental Protection Agency: Washington, DC, USA, 2010. Available online: https://cfpub.epa.gov/ncea/iris/iris_documents/documents/subst/0028_summary.pdf (accessed on 14 March 2026).
46. Su, C.; Zhao, W.; Dong, J.; Yan, X.; Zhong, Y.; Yang, Z. Roof dust accumulation characteristics and influencing factors in typical urban areas of Beijing. *Sci. Rep.* **2025**, *15*, 43645. [CrossRef] [PubMed]
47. *NOM-147-SEMARNAT/SSA1-2004*; Norma Oficial Mexicana, Que Establece Criterios Para la Caracterización y Determinación de Concentraciones de Remediación de Suelos Contaminados por Arsénico, Bario, Berilio, Cadmio, Cromo Hexavalente, Mercurio, Níquel, Plata, Plomo, Selenio, Talio, Vanadio y Sus Compuestos Inorgánicos; Así Como los Criterios de Remediación. Diario Oficial de la Federación: Ciudad de México, Mexico, 2007. Available online: https://www.profepa.gob.mx/innovaportal/file/1392/1/nom-147-semarnat_ssa1-2004.pdf (accessed on 15 March 2026).
48. Adimalla, N. Heavy metals contamination in urban surface soils of Medak province, India, and its risk assessment and spatial distribution. *Environ. Geochem. Health* **2020**, *42*, 59–75. [CrossRef] [PubMed]
49. Dutch Ministry of Housing, Spatial Planning and Environment (VROM). *Circular on Target Values and Intervention Values for Soil Remediation*; Ministerie van Volkshuisvesting, Ruimtelijke Ordening en Milieubeheer: The Hague, The Netherlands, 2000. Available online: https://support.esdat.net/Environmental%20Standards/dutch/annexs_i2000dutch%20environmental%20standards.pdf (accessed on 10 June 2026).
50. Bukowiecki, N.; Lienemann, P.; Hill, M.; Figi, R.; Richard, A.; Furger, M.; Rickers, K.; Falkenberg, G.; Zhao, Y.; Cliff, S.S.; et al. Real-world emission factors for antimony and other brake wear related trace elements: Size-segregated values for light and heavy duty vehicles. *Environ. Sci. Technol.* **2009**, *43*, 8072–8078. [CrossRef] [PubMed]
51. Földi, C.; Sauermann, S.; Dohrmann, R.; Mansfeldt, T. Traffic-related distribution of antimony in roadside soils. *Environ. Pollut.* **2018**, *237*, 704–712. [CrossRef] [PubMed]
52. Gunawardena, J.; Ziyath, A.M.; Egodawatta, P.; Ayoko, G.A.; Goonetilleke, A. Sources and transport pathways of common heavy metals to urban road surfaces. *Ecol. Eng.* **2015**, *77*, 98–102. [CrossRef]
53. Cui, Q.; Brandt, N.; Sinha, R.; Malmström, M.E. Copper content in lake sediments as a tracer of urban emissions: Evaluation through a source–transport–storage model. *Sci. Total Environ.* **2010**, *408*, 2714–2725. [CrossRef] [PubMed]

54. Dousova, B.; Lhotka, M.; Buzek, F.; Cejkova, B.; Jackova, I.; Bednar, V.; Hajek, P. Environmental interaction of antimony and arsenic near busy traffic nodes. *Sci. Total Environ.* **2020**, *702*, 134642. [CrossRef] [PubMed]
55. Ye, J.; Li, J.; Wang, P.; Ning, Y.; Liu, J.; Yu, Q.; Bi, X. Inputs and sources of Pb and other metals in urban area in the post leaded gasoline era. *Environ. Pollut.* **2022**, *306*, 119389. [CrossRef] [PubMed]
56. Yu, A.; Yang, Q.; Xu, B.; Yang, Y.; Ren, Z.; Li, K. Analysis of lead contamination sources in roadside soil via the isotope tracing method. *J. Environ. Chem. Eng.* **2024**, *12*, 114205. [CrossRef]
57. Tume, P.; González, E.; King, R.; Cornejo, Ó.; Wikee, E.; Colima, N.; Roca, N.; Bech, J.; Sepúlveda, B. Assessment of arsenic and mercury contamination in urban soils of Talcahuano, Chile, and their implications for sustainable city planning and public health protection. *Sustainability* **2026**, *18*, 2794. [CrossRef]
58. Hernandez, H.; Rodriguez, R. Geochemical evidence for the origin of vanadium in an urban environment. *Environ. Monit. Assess.* **2012**, *184*, 5327–5342. [CrossRef] [PubMed]
59. Bai, X.; Luo, L.; Tian, H.; Liu, S.; Hao, Y.; Zhao, S.; Lin, S.; Zhu, C.; Guo, Z.; Lv, Y. Atmospheric vanadium emission inventory from both anthropogenic and natural sources in China. *Environ. Sci. Technol.* **2021**, *55*, 11568–11578. [CrossRef] [PubMed]
60. Byrne, P.; Taylor, K.G.; Hudson-Edwards, K.A.; Barrett, J.E.S. Speciation and potential long-term behaviour of chromium in urban sediment particulates. *J. Soils Sediments* **2017**, *17*, 2666–2676. [CrossRef]
61. Bravo-Alvarez, H.; Torres-Jardón, R. Air pollution levels and trends in the Mexico City Metropolitan Area. In *Urban Air Pollution and Forests*; Fenn, M.E., de Bauer, L.I., Hernández-Tejeda, T., Eds.; Ecological Studies; Springer: New York, NY, USA, 2002; Volume 156, pp. 121–159. [CrossRef]
62. Godínez Cárdenas, H.M.; Miranda Pérez, A.F.; Ramírez Portilla, A.; Lezama León, M.H. Environmental simulation model using system dynamics to estimate air pollution: A case study of Mexico City Metropolitan Area. *Sustainability* **2024**, *16*, 8359. [CrossRef]
63. Das, R.; Khezri, B.; Srivastava, B.; Datta, S.; Sikdar, P.K.; Webster, R.D.; Wang, X. Trace element composition of PM2.5 and PM10 from Kolkata—a heavily polluted Indian metropolis. *Atmos. Pollut. Res.* **2015**, *6*, 742–750. [CrossRef]
64. Chang, X.; Li, Y.-X. Lead distribution in urban street dust and the relationship with mining, gross domestic product (GDP), and transportation and health risk assessment. *Environ. Pollut.* **2020**, *262*, 114307. [CrossRef] [PubMed]
65. Zhao, X.; Li, Z.; Tao, Y.; Wang, D.; Huang, J.; Qiao, F.; Lei, L.; Xing, Q. Distribution characteristics, source appointment, and health risk assessment of Cd exposure via household dust in six cities of China. *Build. Environ.* **2020**, *172*, 106728. [CrossRef]
66. Kabata-Pendias, A. *Trace Elements in Soils and Plants*, 4th ed.; CRC Press: Boca Raton, FL, USA, 2010. [CrossRef]
67. Amato, F.; Pandolfi, M.; Moreno, T.; Furger, M.; Pey, J.; Alastuey, A.; Bukowiecki, N.; Prevot, A.S.H.; Baltensperger, U.; Querol, X. Sources and variability of inhalable road dust particles in three European cities. *Atmos. Environ.* **2011**, *45*, 6777–6787. [CrossRef]
68. Iijima, A.; Sato, K.; Yano, K.; Tago, H.; Kato, M.; Kimura, H.; Furuta, N. Particle size and composition distribution analysis of automotive brake abrasion dusts for the evaluation of antimony sources of airborne particulate matter. *Atmos. Environ.* **2007**, *41*, 4908–4919. [CrossRef]
69. Lin, C.-C.; Chen, S.-J.; Huang, K.-L.; Hwang, W.-I.; Chang-Chien, G.-P.; Lin, W.-Y. Characteristics of metals in nano/ultrafine/fine/coarse particles collected beside a heavily trafficked road. *Environ. Sci. Technol.* **2005**, *39*, 8113–8122. [CrossRef] [PubMed]
70. Sternbeck, J.; Sjödin, Å.; Andréasson, K. Metal emissions from road traffic and the influence of resuspension—Results from two tunnel studies. *Atmos. Environ.* **2002**, *36*, 4735–4744. [CrossRef]
71. Jeong, H.; Ryu, J.-S.; Ra, K. Characteristics of potentially toxic elements and multi-isotope signatures (Cu, Zn, Pb) in non-exhaust traffic emission sources. *Environ. Pollut.* **2022**, *292*, 118339. [CrossRef] [PubMed]
72. Wagner, S.; Funk, C.W.; Müller, K.; Raithel, D.J. The chemical composition and sources of road dust, and of tire and road wear particles: A review. *Sci. Total Environ.* **2024**, *926*, 171694. [CrossRef] [PubMed]
73. Manigrasso, M.; Protano, C.; Martellucci, S.; Mattei, V.; Vitali, M.; Avino, P. Evaluation of the submicron particles distribution between mountain and urban site: Contribution of the transportation for defining environmental and human health issues. *Int. J. Environ. Res. Public Health* **2019**, *16*, 1339. [CrossRef] [PubMed]
74. Schiavo, B.; Morton-Bermea, O.; Meza-Figueroa, D.; Acosta-Elías, M.; González-Grijalva, B.; Armienta-Hernández, M.A.; Inguaggiato, C.; Valera-Fernández, D. Characterization and polydispersity of volcanic ash nanoparticles in synthetic lung fluid. *Toxics* **2023**, *11*, 624. [CrossRef] [PubMed]
75. Kelly, F.J.; Fussell, J.C. Size, source and chemical composition as determinants of toxicity attributable to ambient particulate matter. *Atmos. Environ.* **2012**, *60*, 504–526. [CrossRef]
76. Adachi, K.; Tainosho, Y. Characterization of heavy metal particles embedded in tire dust. *Environ. Int.* **2004**, *30*, 1009–1017. [CrossRef] [PubMed]
77. Thorpe, A.; Harrison, R.M. Sources and properties of non-exhaust particulate matter from road traffic: A review. *Sci. Total Environ.* **2008**, *400*, 270–282. [CrossRef] [PubMed]
78. Guney, M.; Onay, T.T.; Copty, N.K. Impact of overland traffic on heavy metal levels in highway dust and soils of Istanbul, Turkey. *Environ. Monit. Assess.* **2010**, *164*, 101–110. [CrossRef] [PubMed]

79. Grigoratos, T.; Martini, G. Brake wear particle emissions: A review. *Environ. Sci. Pollut. Res.* **2015**, *22*, 2491–2504. [CrossRef] [PubMed]
80. Kole, P.J.; Löhr, A.J.; Van Belleghem, F.G.A.J.; Ragas, A.M.J. Wear and tear of tyres: A stealthy source of microplastics in the environment. *Int. J. Environ. Res. Public Health* **2017**, *14*, 1265. [CrossRef] [PubMed]
81. Sommer, F.; Dietze, V.; Baum, A.; Sauer, J.; Gilge, S.; Maschowski, C.; Gieré, R. Tire abrasion as a major source of microplastics in the environment. *Aerosol Air Qual. Res.* **2018**, *18*, 2014–2028. [CrossRef]
82. Birgül, A. Assessing heavy metal contamination and health risks in playground dust near cement factory: Exposure levels in children. *Environ. Geochem. Health* **2024**, *46*, 368. [CrossRef] [PubMed]
83. Utembe, W. Issues around the deterministic reference dose for lead and human safety concerns regarding its continued utilization. *Curr. Opin. Toxicol.* **2025**, *44*, 100549. [CrossRef]
84. Hernández-Pellón, A.; Nischkauer, W.; Limbeck, A.; Fernández-Olmo, I. Metal(loid) bioaccessibility and inhalation risk assessment: A comparison between an urban and an industrial area. *Environ. Res.* **2018**, *165*, 140–149. [CrossRef] [PubMed]
85. Wiseman, C.L.S.; Niu, J.; Levesque, C.; Chénier, M.; Rasmussen, P.E. An assessment of the inhalation bioaccessibility of platinum group elements in road dust using a simulated lung fluid. *Environ. Pollut.* **2018**, *241*, 1009–1017. [CrossRef] [PubMed]

Disclaimer/Publisher's Note: The statements, opinions and data contained in all publications are solely those of the individual author(s) and contributor(s) and not of MDPI and/or the editor(s). MDPI and/or the editor(s) disclaim responsibility for any injury to people or property resulting from any ideas, methods, instructions or products referred to in the content.